Astron. Astrophys. 186, 49–63 (1987)

ASTRONOMY
AND
ASTROPHYSICS

# Near-infrared spectral properties of star clusters and galactic nuclei*

**E. Bica and D. Alloin**

Observatoire de Paris, Section de Meudon, F-92195 Meudon Principal Cedex, France

Received January 6, accepted February 23, 1987

**Summary.** We present CCD spectra with 12.5 Å resolution from 6300 to 9700 Å of 30 star clusters covering ranges $10^6$ to 1.65 $10^{10}$ yr in age, and $-2.0$ to 0.1 in metallicity, $[Z/Z_\odot]$. As well, 62 galactic nuclei have been observed in galaxies with morphological types E to Sc and intrinsic luminosities $-23.3 \leqq M_B \leqq -16.7$. For every object in the present sample, the visible spectrum has been discussed in earlier papers. We describe a powerful method for correcting CCD fringes in the near-infrared. We measure the near-infrared continuum distribution and the equivalent widths (W) of 13 absorption features. Analysis of the star cluster sample indicates that in the near-infrared spectral range, metallicity is the dominant parameter. Age produces second order effects of various types: (i) enhancement of molecular bands in certain phases of a blue cluster evolution by the accumulation of luminous red stars, (ii) contamination of metallic lines with Paschen absorption lines and, (iii) slight steepening of the continuum slope for young clusters. In view of population synthesis of galactic nuclei using the star clusters, we present grid predictions as a function of metallicity and age for 5 metallic features and for the continuum distribution. Spiral galaxies and luminous elliptical galaxies show similar strong-lined spectra suggesting that their metallicities in the central regions are comparable. Even very blue galaxies exhibit in the near-infrared spectra quite similar to those of more classical galaxies. Evidence is found however that a large flux contribution to this range is not from their old underlying population. Strong-lined globular clusters like NGC 6528 have integrated spectra comparable to those of massive galaxies. Consequently, they are of a great help in population synthesis work, whatever their precise metallicity value.

**Key words:** near-infrared spectra – star clusters – galactic nuclei

## 1. Introduction

As yet much effort has been devoted to the interpretation of near-infrared feature strengths in the spectra of galactic nuclei, in terms of the stellar types which contribute most to their integrated light (e.g. Spinrad and Taylor, 1971; Turnrose, 1976; Cohen, 1979; Faber and French, 1980; Jones et al., 1984; Carter et al., 1986). These studies also showed how the Ca II triplet (8498, 8542, 8662 Å), the Na I 8190 Å line and various molecular bands depend on gravity, temperature and metallicity of stars, the latter parameter being in general restricted to 0.5 dex around the solar value. We shall undertake a similar analysis for our sample of galactic nuclear spectra studying them in the light of stellar properties in a forthcoming paper.

The aim of the present work is, on the other hand, to analyze features in galactic nuclear spectra as a function of those observed in the integrated spectra of a sample of star clusters with known age, metallicity and reddening. This new approach is part of a population synthesis program over a wide spectral domain. The library of star cluster integrated spectra covers a large range in age and metallicity. This method offers the advantage over the one using stellar libraries, of being a two-parameter analysis (Bica and Alloin, 1986a, hereafter Paper I). The present approach constitutes in turn, an intermediate step towards a deeper insight into the stellar content itself of galactic nuclei since the HR diagrams of the star clusters are known from independent studies.

The observations are presented in Sect. 2. We describe also in this section, the CCD reduction procedure, in particular the removal of interference fringes and the correction of atmospheric absorption bands. In Sect. 3 we identify absorption features, we discuss criteria for continuum tracings and we define windows for equivalent width measurements W to be used in the synthesis. We study in Sect. 4 the star cluster properties as a function of age and metallicity. Results for galactic nuclei are examined in Sect. 5, as a function of morphological type and intrinsic luminosity of the parent galaxy. Conclusions of this work are given in Sect. 6. In Appendix A, we present grid predictions for equivalent widths (W) and continuum distribution of star clusters as a function of age and metallicity $[Z/Z_\odot]$, following the grid already obtained in the visible range (Bica and Alloin, 1986b, hereafter Paper II).

## 2. Observational data and reduction procedure

### 2.1. The sample

We observed 30 star clusters and 62 galactic nuclei for which a visible spectrum had already been obtained and discussed in Paper I and Papers III, IV (Bica and Alloin, 1987a, b). The present sample is a subset of the visible one, about a half; nevertheless, we still cover for star clusters the same ranges in age from $10^6$ to 1.65 $10^{10}$ yr and in metallicity $-2.0 \leqq [Z/Z_\odot] \leqq 0.1$, and, for galaxies the same ranges in intrinsic luminosity $-23.3 \leqq M_B \leqq -16.7$ and in morphological types from E to Sc. The star clusters are listed in Table 1 and the galaxies in Table 2, while their basic parameters have been compiled in Papers I and III respectively.

*Send offprint requests to:* D. Alloin

* Based upon observational data collected at the European Southern Observatory

**Table 1.** Col. (10), (12), and (16): The values correspond to a low continuum tracing with the aim of minimizing molecular contamination in the Ca II windows (Sect. 3). Symbol id. means that the measurement is identical to that in the preceeding column. Col. (19)–(25): Continuum points, expressed in $F_\lambda$ units, are corrected for reddening according to Sect. 3 and are normalized to the value at $\lambda = 5870$ Å

| (1) | (2) | (3) | (4) | (5) | (6) | (7) | (8) | (9) | (10) | (11) | (12) | (13) |
|---|---|---|---|---|---|---|---|---|---|---|---|---|
| NGC | #59 | #60 | #66/7/8 | #71 | #72 | #74 | #75/6 | #77 | #77 | #78 | #78 | #79 |
| | CaI | Hα | TiO | TiO | CN | NaI | TiO | CaII | CaII | CaII | CaII | P14 |
| | FeI | | | | | | TiI | TiO | | TiO | | TiO |
| **Large Magellanic Cloud Clusters** | | | | | | | | | | | | |
| 1714 | 0 | -1370 | -103 | -26 | 0 | 0 | 0 | 0 | 0 | 0 | 0 | 0 |
| 1783 | 0.4 | 2.9 | 18.3 | 5.5 | 2.5 | 1.3 | 4.5 | 2.5 | id. | 4.0 | id. | 1.0 |
| 1831 | 0.4 | 7.3 | 5.1 | 0.0 | 6.2 | 0.9 | 13.4 | 0.4 | id. | 4.8 | id. | 1.9 |
| 1847 | 0.7 | 1.8 | 11.9 | 2.9 | 5.1 | 2.7 | 9.0 | 2.8 | id. | 4.6 | id. | 1.4 |
| 1856 | 0.7 | 5.5 | 8.7 | 2.1 | 4.3 | 2.6 | 9.2 | 2.1 | id. | 4.1 | id. | 1.1 |
| 1866 | 1.1 | 3.8 | 25.8 | 15.0 | 12.4 | 0.9 | 10.3 | 4.3 | 3.1 | 5.5 | 4.6 | 3.9 |
| 1868 | 0.4 | 5.2 | 4.6 | 2.1 | 4.2 | 1.3 | 7.7 | 1.9 | id. | 3.5 | id. | 1.3 |
| 1978 | 0.9 | 3.6 | 14.2 | 0.0 | 5.2 | 1.4 | 8.8 | 0.7 | id. | 3.1 | id. | 0.8 |
| 2004 | 2.5 | 0.0 | 34.8 | 3.6 | 6.4 | 1.8 | 11.1 | 3.2 | 2.3 | 6.1 | 5.4 | 1.7 |
| 2157 | 0.3 | 2.6 | 8.1 | 1.4 | 2.2 | 1.6 | 7.5 | 1.5 | id. | 4.0 | id. | 1.2 |
| 2214 | 0.8 | -3.3 | 15.4 | 0.9 | 5.4 | 0.3 | 3.8 | 1.6 | id. | 4.1 | id. | 1.2 |
| **Galactic Globular Clusters** | | | | | | | | | | | | |
| 5024 | 0.3 | 2.7 | 0.0 | 0.5 | 0.6 | 0.3 | 2.2 | 0.7 | id. | 1.4 | id. | 0.1 |
| 5824 | 0.6 | 2.7 | 1.9 | 0.2 | 0.3 | 0.5 | 1.6 | 0.8 | id. | 1.9 | id. | 0.4 |
| 5927 | 1.5 | 2.6 | 26.8 | 8.2 | 6.9 | 1.7 | 11.9 | 4.6 | 3.1 | 5.8 | 4.5 | 4.3 |
| 6093 | 0.2 | 2.6 | 2.4 | 1.2 | 1.2 | 1.8 | 3.9 | 1.2 | id. | 2.4 | id. | 1.1 |
| 6293 | 0.4 | 2.4 | 0.7 | 1.9 | 1.3 | 0.7 | 2.4 | 0.9 | id. | 1.4 | id. | 0.3 |
| 6316 | 0.8 | 1.8 | 11.7 | 4.7 | 3.4 | 2.2 | 10.2 | 2.5 | id. | 4.2 | id. | 1.8 |
| 6356 | 0.6 | 2.0 | 9.5 | 1.0 | 2.3 | 1.2 | 5.3 | 1.9 | id. | 3.5 | id. | 0.6 |
| 6388 | 0.6 | 1.7 | 13.8 | 2.6 | 2.5 | 1.6 | 8.6 | 3.0 | id. | 4.4 | id. | 2.4 |
| 6440 | 1.1 | 2.2 | 21.4 | 9.2 | 7.9 | 1.8 | 14.8 | 4.4 | 2.5 | 5.8 | 4.1 | 4.4 |
| 6453 | 0.7 | 2.3 | 2.5 | 3.6 | 1.6 | 1.5 | 5.4 | 1.4 | id. | 2.5 | id. | 1.8 |
| 6528 | 2.1 | 2.7 | 38.6 | 14.5 | 12.4 | 2.3 | 18.2 | 5.7 | 3.3 | 7.4 | 5.4 | 5.9 |
| 6624 | 1.2 | 2.5 | 25.0 | 9.9 | 7.9 | 1.9 | 12.6 | 3.9 | 2.6 | 5.4 | 4.3 | 3.3 |
| 6638 | 0.4 | 1.8 | 5.3 | 1.0 | 1.3 | 1.1 | 4.7 | 1.6 | id. | 2.9 | id. | 0.3 |
| 6642 | 1.1 | 2.8 | 4.3 | 1.5 | 1.7 | 0.6 | 4.4 | 1.7 | id. | 2.6 | id. | 0.0 |
| 6652 | 0.3 | 2.4 | 2.7 | 0.3 | 1.3 | 1.4 | 4.2 | 1.7 | id. | 2.9 | id. | 0.5 |
| 6715 | 0.3 | 2.5 | 5.2 | 3.6 | 4.6 | 0.9 | 3.8 | 2.1 | id. | 3.8 | id. | 1.4 |
| 6864 | 0.4 | 2.4 | 1.7 | 1.0 | 1.7 | 0.6 | 2.6 | 1.6 | id. | 3.0 | id. | 0.8 |
| **Galactic Open Clusters** | | | | | | | | | | | | |
| 2660 | 0.5 | 3.9 | 17.1 | 6.0 | 4.3 | 1.7 | 8.2 | 1.6 | id. | 2.8 | id. | 2.0 |
| 6705 | 1.1 | 5.5 | 8.3 | 0.9 | 3.8 | 1.8 | 6.6 | 2.1 | id. | 3.7 | id. | 2.6 |

| (14) | (15) | (16) | (17) | (18) | (19) | (20) | (21) | (22) | (23) | (24) | (25) |
|---|---|---|---|---|---|---|---|---|---|---|---|
| NGC | #80 | #80 | #81 | #83/84 | Cont | Cont | Cont | Cont | Cont | Cont | Cont |
| | CaII | CaII | P12 | TiO | 6630 | 6990 | 7520 | 8040 | 8408 | 8700 | 9100 |
| | TiO | | FeI | P11+10 | 5870 | 5870 | 5870 | 5870 | 5870 | 5870 | 5870 |
| **Large Magellanic Cloud Clusters** | | | | | | | | | | | |
| 1714 | -5 | 0 | -11 | -22 | 0.76 | 0.69 | 0.61 | 0.49 | 0.44 | 0.41 | 0.37 |
| 1783 | 4.9 | id. | 1.6 | 8.8 | 0.93 | 0.91 | 0.86 | 0.81 | 0.76 | 0.76 | 0.75 |
| 1831 | 6.1 | id. | 5.1 | 12.8 | 0.79 | 0.72 | 0.63 | 0.57 | 0.52 | 0.50 | 0.49 |
| 1847 | 5.8 | id. | 3.2 | 13.1 | 0.80 | 0.73 | 0.67 | 0.61 | 0.58 | 0.61 | 0.56 |
| 1856 | 4.3 | id. | 2.1 | 11.6 | 0.77 | 0.71 | 0.64 | 0.58 | 0.54 | 0.54 | 0.50 |
| 1866 | 5.3 | 4.8 | 2.6 | 14.6 | 0.90 | 0.84 | 0.81 | 0.75 | 0.71 | 0.71 | 0.68 |
| 1868 | 3.9 | id. | 1.9 | 10.1 | 0.91 | 0.83 | 0.76 | 0.70 | 0.66 | 0.65 | 0.61 |
| 1978 | 2.9 | id. | 1.9 | 4.5 | 1.10 | 1.07 | 1.01 | 0.94 | 0.89 | 0.90 | 0.85 |
| 2004 | 5.2 | 4.8 | 1.2 | 6.9 | 0.96 | 0.96 | 0.93 | 0.94 | 0.93 | 0.94 | 0.92 |
| 2157 | 4.3 | id. | 1.4 | 9.6 | 0.88 | 0.79 | 0.71 | 0.63 | 0.59 | 0.58 | 0.54 |
| 2214 | 4.9 | id. | 0.9 | 16.2 | 0.89 | 0.81 | 0.73 | 0.65 | 0.61 | 0.61 | 0.58 |
| **Galactic Globular Clusters** | | | | | | | | | | | |
| 5024 | 1.8 | id. | 0.7 | 3.5 | 0.92 | 0.86 | 0.81 | 0.77 | 0.73 | 0.71 | 0.69 |
| 5824 | 2.0 | id. | 0.0 | 2.0 | 0.92 | 0.89 | 0.84 | 0.80 | 0.76 | 0.76 | 0.73 |
| 5927 | 5.2 | 4.2 | 2.8 | 8.4 | 0.96 | 0.95 | 0.93 | 0.92 | 0.92 | 0.92 | 0.91 |
| 6093 | 2.2 | id. | 0.4 | 3.7 | 0.95 | 0.91 | 0.86 | 0.82 | 0.79 | 0.79 | 0.77 |
| 6293 | 2.0 | id. | 0.4 | 4.5 | 0.87 | 0.84 | 0.81 | 0.78 | 0.74 | 0.74 | 0.71 |
| 6316 | 4.1 | id. | 1.1 | 3.7 | 0.94 | 0.94 | 0.94 | 0.93 | 0.92 | 0.92 | 0.89 |
| 6356 | 3.5 | id. | 1.0 | 2.4 | 0.90 | 0.89 | 0.88 | 0.85 | 0.83 | 0.83 | 0.80 |
| 6388 | 3.9 | id. | 1.7 | 3.5 | 0.97 | 0.95 | 0.91 | 0.90 | 0.90 | 0.89 | 0.88 |
| 6440 | 5.5 | 3.9 | 2.7 | 6.7 | 1.07 | 1.10 | 1.13 | 1.16 | 1.18 | 1.20 | 1.21 |
| 6453 | 3.0 | id. | 0.3 | 5.1 | 0.95 | 0.93 | 0.89 | 0.86 | 0.84 | 0.84 | 0.81 |
| 6528 | 6.3 | 4.5 | 2.4 | 9.3 | 0.94 | 0.96 | 0.98 | 0.97 | 0.97 | 0.99 | 1.00 |
| 6624 | 4.4 | 3.8 | 0.8 | 5.2 | 0.89 | 0.89 | 0.91 | 0.88 | 0.87 | 0.87 | 0.85 |
| 6638 | 3.0 | id. | 0.1 | 1.9 | 0.91 | 0.89 | 0.89 | 0.86 | 0.84 | 0.84 | 0.80 |
| 6642 | 3.0 | id. | 0.4 | 3.3 | 1.02 | 1.00 | 0.98 | 0.95 | 0.93 | 0.93 | 0.90 |
| 6652 | 3.2 | id. | 0.7 | 4.9 | 0.88 | 0.86 | 0.81 | 0.77 | 0.74 | 0.74 | 0.70 |
| 6715 | 3.1 | id. | 0.6 | 5.2 | 0.93 | 0.87 | 0.82 | 0.79 | 0.74 | 0.75 | 0.73 |
| 6864 | 3.0 | id. | 1.1 | 2.6 | 0.96 | 0.90 | 0.84 | 0.80 | 0.76 | 0.74 | 0.71 |
| **Galactic Open Clusters** | | | | | | | | | | | |
| 2660 | 4.4 | id. | 3.3 | 10.6 | 0.82 | 0.78 | 0.72 | 0.66 | 0.63 | 0.62 | 0.61 |
| 6705 | 4.5 | id. | 3.4 | 8.7 | 0.75 | 0.67 | 0.58 | 0.52 | 0.48 | 0.48 | 0.47 |

The observations were carried out from 1985 April 29 to May 3, with the 2.2 m telescope at ESO, La Silla. We used a CCD attached to the Boller and Chivens spectrograph with a 300 lines/mm grating in first order providing a dispersion 228 Å mm$^{-1}$, and an OG 590 filter so as to eliminate the second order contamination. The CCD array (RCA thinned, backside illuminated) consists of 512 pixels along the dispersion, by 320 pixels of which the central 120 were illuminated by the slit length. A 30 μm square pixel corresponds to 1″.8 on the sky and 6 Å along the dispersion. The spectral resolution, as measured by the FWHM of helium-argon comparison lines is of 12.5 Å. In order to get a spectral resolution similar to that achieved in the visible range, we had to keep a 2″.5 slit width, narrower than the 4″ to 5″ slit previously employed. This procedure did not introduce however, significant or systematic differences in the spectra of galactic nuclei, as demonstrated by the comparison of the 1000 Å overlap between the two domains. For each galaxy we summed the pixel rows perpendicular to the dispersion in order to match the slit lengths used for observations in the visible. These values (in arc sec) and the corresponding dimensions at the source can be found in Paper III.

The slit was generally set E–W, but for galaxies presenting a preferential axis, particular orientations were chosen in view of a future spatial analysis of some absorption features. For instance, in edge-on spirals and lenticulars, the slit length was set along the minor axis. Star clusters were scanned spatially in the dispersion direction and we summed pixel rows along the slit length in order to reproduce the areas which had been looked at in the visible data as specified in Paper I. For large clusters a separate frame for the sky was considered. Owing to the strong night sky emission lines in the near-infrared range, these cases were given special attention in order to ensure a satisfactory sky cancellation.

### 2.2. *Reduction procedure*

The reductions were carried out with the IHAP system at ESO Garching and Institut d'Astrophysique de Paris. The CCD reduction procedure consisted of:

(i) removal of the dark current bias;
(ii) flat-fielding;
(iii) object and sky compression to one dimension;
(iv) sky subtraction and wavelength calibration;
(v) correction for atmospheric extinction and flux calibration;
(vi) removal of atmospheric absorption bands.

Items (ii) and (vi) deserve a more detailed description.

The presence of fringes in near-infrared CCD spectra is a well known problem. Normally these fringes should be removed through a standard division by the flat field frame (FFF).

**Table 2.** Col. (1): An asterisk denotes IC galaxies. Col. (4): Correction for emission line contamination was applied to NGC 5643. Cols. (10), (12), and (16): The values correspond to a low continuum tracing with the aim of minimizing molecular contamination in the Ca II windows (Sect. 3). Symbol id. means that the measurement is identical to that in the preceeding column. Cols. (19)–(25): Continuum points, expressed in $F_\lambda$ units, are corrected for reddening according to Sect. 3 and are normalized to the value at $\lambda = 5870$ Å

| (1) NGC | (2) #59 CaI FeI | (3) #60 Hα | (4) #66/7/8 TiO | (5) #71 TiO | (6) #72 CN | (7) #74 NaI | (8) #75/6 TiO TiI | (9) #77 CaII TiO | (10) #77 CaII | (11) #78 CaII TiO | (12) #78 CaII | (13) #79 P14 TiO |
|---|---|---|---|---|---|---|---|---|---|---|---|---|
| | E I' | | -22.7 < M < -22.0 | | | | | | | | | |
| 4296* | 0.6 | -0.8 | 26.8 | 7.1 | 7.6 | 2.1 | 10.7 | 4.3 | 3.0 | 5.4 | 4.3 | 2.9 |
| 3557 | 1.2 | 1.1 | 30.2 | 6.6 | 8.3 | 3.1 | 11.3 | 4.5 | 3.0 | 6.3 | 5.0 | 3.7 |
| 6776 | 0.5 | -1.9 | 22.2 | 6.6 | 7.5 | 2.8 | 12.3 | 3.8 | 2.0 | 6.0 | 4.6 | 2.6 |
| | E II' | | -21.9 < M < -21.0 | | | | | | | | | |
| 5018 | 0.5 | 0.6 | 20.1 | 4.4 | 4.3 | 1.8 | 10.8 | 4.4 | 2.9 | 5.7 | 4.4 | 2.4 |
| 4936 | 0.7 | -4.9 | 23.9 | 7.4 | 7.8 | 1.6 | 13.3 | 4.6 | 2.9 | 5.9 | 4.5 | 3.9 |
| 6758 | 1.2 | -0.6 | 27.6 | 6.6 | 7.2 | 1.2 | 10.6 | 3.5 | 2.2 | 4.7 | 3.6 | 2.2 |
| 5061 | 1.3 | 1.7 | 27.0 | 5.6 | 5.5 | 2.2 | 12.5 | 4.4 | 2.7 | 5.7 | 4.3 | 3.3 |
| 4697 | 3.4 | 2.6 | 33.4 | 8.4 | 8.3 | 2.3 | 14.5 | 4.7 | 2.8 | 5.8 | 4.2 | 2.4 |
| 2865 | 1.2 | 2.5 | 19.8 | 4.6 | 7.0 | 2.3 | 9.9 | 3.5 | 2.6 | 5.3 | 4.5 | 2.6 |
| 7144 | 0.8 | 2.1 | 25.9 | 8.5 | 9.4 | 1.9 | 15.7 | 4.7 | 2.9 | 5.8 | 4.3 | 4.2 |
| | E III' | | -20.9 < M < -19.0 | | | | | | | | | |
| 7145 | 0.7 | 2.3 | 25.6 | 8.8 | 10.0 | 2.5 | 16.8 | 5.0 | 3.0 | 6.5 | 4.8 | 4.5 |
| 3904 | 1.1 | 2.3 | 27.0 | 9.1 | 9.5 | 2.1 | 15.2 | 4.4 | 2.7 | 6.1 | 4.7 | 4.2 |
| 2434 | 0.9 | 1.3 | 26.7 | 9.2 | 9.8 | 1.8 | 15.7 | 4.9 | 3.3 | 6.8 | 5.5 | 3.7 |
| 4742 | 1.1 | 2.7 | 23.0 | 6.2 | 6.6 | 1.7 | 14.2 | 4.7 | 2.7 | 5.7 | 4.1 | 3.8 |
| 4478 | 1.3 | 2.9 | 23.6 | 7.8 | 9.0 | 3.0 | 14.5 | 3.7 | 2.1 | 5.3 | 3.9 | 5.8 |
| 3818 | 1.7 | 1.8 | 27.1 | 7.5 | 7.0 | 2.3 | 11.5 | 4.7 | 2.8 | 5.3 | 3.6 | 3.3 |
| | E IV' | | -18.9 < M < -16.5 | | | | | | | | | |
| 4486B | 1.5 | 2.1 | 25.7 | 7.4 | 8.7 | 1.6 | 11.8 | 4.2 | 3.0 | 5.5 | 4.6 | 4.9 |
| | S0 I' | | -22.3 < M < -22.0 | | | | | | | | | |
| 5419 | 1.5 | 1.8 | 29.6 | 7.4 | 7.5 | 1.7 | 11.9 | 4.1 | 2.6 | 4.9 | 3.6 | 2.7 |
| | S0 II' | | -21.9 < M < -21.0 | | | | | | | | | |
| 6868 | 1.0 | -4.0 | 27.2 | 7.3 | 8.6 | 2.7 | 12.8 | 4.7 | 3.3 | 5.8 | 4.6 | 3.4 |
| 5266 | 1.6 | -5.5 | 26.4 | 5.5 | 7.6 | 2.0 | 10.2 | 4.1 | 3.3 | 4.6 | 3.9 | 0.9 |
| 6861 | 1.2 | -0.9 | 27.7 | 7.6 | 8.7 | 2.4 | 12.2 | 4.6 | 3.1 | 5.0 | 3.8 | 2.8 |
| 3923 | 1.7 | 2.2 | 28.5 | 7.6 | 9.1 | 2.4 | 12.0 | 4.7 | 3.0 | 6.1 | 4.7 | 3.7 |
| 4797* | 1.4 | 1.6 | 26.7 | 7.0 | 8.9 | 2.5 | 11.8 | 4.8 | 3.4 | 5.8 | 4.6 | 3.2 |
| 4889* | 0.8 | -0.2 | 26.4 | 8.5 | 10.4 | 1.2 | 12.1 | 4.6 | 3.1 | 5.1 | 3.7 | 2.9 |
| 3585 | 1.6 | 2.1 | 29.0 | 7.6 | 9.5 | 2.1 | 12.1 | 5.1 | 3.7 | 5.8 | 4.6 | 3.7 |
| | S0 III' | | -20.9 < M < -19.0 | | | | | | | | | |
| 4976 | 0.9 | 2.2 | 25.6 | 8.4 | 9.8 | 2.2 | 16.3 | 4.5 | 2.6 | 6.5 | 4.9 | 4.1 |
| 7041 | 0.9 | 1.8 | 27.3 | 8.3 | 9.6 | 1.8 | 15.0 | 4.6 | 2.9 | 6.1 | 4.7 | 3.6 |
| 4958 | 0.6 | -1.0 | 26.3 | 7.5 | 8.3 | 2.0 | 13.0 | 4.6 | 3.1 | 6.3 | 5.0 | 3.9 |
| 3115 | 1.3 | 2.2 | 30.7 | 10.2 | 12.9 | 2.3 | 17.4 | 5.1 | 3.2 | 6.8 | 5.3 | 5.6 |
| 4033 | 1.3 | 2.2 | 27.3 | 7.4 | 9.7 | 2.2 | 13.1 | 4.8 | 3.3 | 6.8 | 5.5 | 4.7 |
| | S0 IV' | | -18.9 < M < -18.4 | | | | | | | | | |
| 5102 | 0.6 | 1.9 | 12.4 | 1.3 | 3.6 | 1.7 | 5.8 | 2.5 | id. | 4.6 | id. | 1.6 |
| 3056 | 0.7 | -2.8 | 16.4 | 6.2 | 5.6 | 1.5 | 11.2 | 3.5 | 2.3 | 5.2 | 4.2 | 1.5 |

| (14) NGC | (15) #80 CaII TiO | (16) #80 CaII | (17) #81 P12 FeI | (18) #83/84 TiO P11+10 | (19) Cont 6630 5870 | (20) Cont 6990 5870 | (21) Cont 7520 5870 | (22) Cont 8040 5870 | (23) Cont 8408 5870 | (24) Cont 8700 5870 | (25) Cont 9100 5870 |
|---|---|---|---|---|---|---|---|---|---|---|---|
| | E I' | | -22.7 < M < -22.0 | | | | | | | | |
| 4296* | 3.9 | 3.0 | 2.3 | 6.8 | 1.00 | 0.99 | 1.02 | 1.02 | 1.02 | 1.02 | 1.05 |
| 3557 | 4.2 | 2.9 | 1.3 | 5.6 | 0.99 | 0.99 | 1.01 | 1.00 | 1.00 | 1.00 | 1.02 |
| 6776 | 5.7 | 4.4 | 4.6 | 6.2 | 0.98 | 0.94 | 0.95 | 0.93 | 0.92 | 0.92 | 0.92 |
| | E II' | | -21.9 < M < -21.0 | | | | | | | | |
| 5018 | 4.9 | 3.6 | 2.5 | 3.9 | 1.00 | 0.99 | 0.99 | 0.97 | 0.97 | 0.98 | 0.99 |
| 4936 | 5.4 | 4.1 | 2.7 | 5.9 | 1.05 | 1.05 | 1.12 | 1.13 | 1.15 | 1.16 | 1.20 |
| 6758 | 3.6 | 2.8 | 1.7 | 5.5 | 0.98 | 0.96 | 0.98 | 0.97 | 0.97 | 0.97 | 0.98 |
| 5061 | 5.6 | 4.3 | 3.5 | 7.3 | 0.95 | 0.94 | 0.93 | 0.92 | 0.92 | 0.92 | 0.91 |
| 4697 | 5.9 | 4.3 | 3.5 | 6.6 | 0.97 | 0.99 | 1.00 | 1.01 | 1.02 | 1.03 | 1.04 |
| 2865 | 3.7 | 3.1 | 0.8 | 6.9 | 0.90 | 0.87 | 0.85 | 0.81 | 0.79 | 0.79 | 0.78 |
| 7144 | 6.1 | 4.9 | 3.0 | 8.0 | 1.01 | 0.99 | 1.01 | 0.99 | 0.99 | 0.99 | 0.99 |
| | E III' | | -20.9 < M < -19.0 | | | | | | | | |
| 7145 | 6.2 | 4.8 | 2.8 | 9.7 | 0.99 | 0.98 | 1.00 | 0.99 | 0.99 | 0.99 | 0.98 |
| 3904 | 5.7 | 4.3 | 2.6 | 6.2 | 1.01 | 0.99 | 1.02 | 1.00 | 1.00 | 1.00 | 1.00 |
| 2434 | 5.3 | 4.2 | 1.4 | 13.5 | 1.04 | 1.05 | 1.11 | 1.12 | 1.14 | 1.15 | 1.17 |
| 4742 | 6.3 | 4.9 | 4.5 | 9.3 | 0.94 | 0.91 | 0.89 | 0.87 | 0.87 | 0.86 | 0.85 |
| 4478 | 5.5 | 4.6 | 3.3 | 8.4 | 0.95 | 0.95 | 1.01 | 1.02 | 1.02 | 1.02 | 1.01 |
| 3818 | 4.4 | 3.0 | 3.8 | 4.8 | 0.97 | 0.98 | 0.99 | 1.00 | 1.00 | 1.00 | 1.00 |
| | E IV' | | -18.9 < M < -16.5 | | | | | | | | |
| 4486B | 3.5 | 2.8 | 1.8 | 5.6 | 0.96 | 0.97 | 1.01 | 1.00 | 1.00 | 1.00 | 0.98 |
| | S0 I' | | -22.3 < M < -22.0 | | | | | | | | |
| 5419 | 4.1 | 2.8 | 2.8 | 10.5 | 1.01 | 0.99 | 1.03 | 1.01 | 1.01 | 1.02 | 1.04 |
| | S0 II' | | -21.9 < M < -21.0 | | | | | | | | |
| 6868 | 4.2 | 3.4 | 2.1 | 7.3 | 1.03 | 1.03 | 1.06 | 1.06 | 1.07 | 1.07 | 1.10 |
| 5266 | 3.0 | 2.7 | 0.0 | 7.6 | 1.02 | 1.04 | 1.09 | 1.08 | 1.08 | 1.09 | 1.11 |
| 6861 | 4.0 | 3.2 | 1.8 | 5.3 | 1.06 | 1.06 | 1.09 | 1.09 | 1.09 | 1.09 | 1.11 |
| 3923 | 4.3 | 3.0 | 2.4 | 5.2 | 0.99 | 1.01 | 1.07 | 1.06 | 1.06 | 1.07 | 1.07 |
| 4797* | 4.8 | 3.7 | 2.2 | 6.1 | 0.96 | 0.95 | 0.98 | 0.97 | 0.97 | 0.98 | 1.00 |
| 4889* | 5.0 | 3.8 | 1.6 | 12.6 | 0.96 | 0.95 | 0.97 | 0.94 | 0.93 | 0.94 | 0.93 |
| 3585 | 4.5 | 3.4 | 2.6 | 4.9 | 0.97 | 0.97 | 1.02 | 0.99 | 0.99 | 1.00 | 0.99 |
| | S0 III' | | -20.9 < M < -19.0 | | | | | | | | |
| 4976 | 5.6 | 4.1 | 2.9 | 7.6 | 0.99 | 0.97 | 0.99 | 0.97 | 0.97 | 0.97 | 0.96 |
| 7041 | 4.6 | 3.4 | 1.7 | 7.5 | 1.00 | 1.02 | 1.07 | 1.06 | 1.06 | 1.05 | 1.03 |
| 4958 | 4.9 | 3.7 | 2.3 | 3.7 | 0.94 | 0.94 | 0.96 | 0.95 | 0.95 | 0.96 | 0.96 |
| 3115 | 6.0 | 4.7 | 2.4 | 9.8 | 1.02 | 0.99 | 1.04 | 1.03 | 1.03 | 1.02 | 1.03 |
| 4033 | 5.4 | 4.2 | 2.1 | 7.9 | 0.97 | 0.96 | 0.97 | 0.95 | 0.95 | 0.94 | 0.94 |
| | S0 IV' | | -18.9 < M < -18.4 | | | | | | | | |
| 5102 | 3.9 | id. | 1.5 | 7.1 | 0.92 | 0.86 | 0.81 | 0.76 | 0.72 | 0.72 | 0.69 |
| 3056 | 4.7 | 3.9 | 1.7 | 5.7 | 0.96 | 0.93 | 0.94 | 0.92 | 0.91 | 0.90 | 0.89 |

However this was not so in our spectra where we verified that the fringe systems in the FFF and in the scientific frame (SF) might present relative shifts up to 1.5 pixels along the dispersion, most probably as a result of flexures. Furthermore, the fringe intensities in the SF were around 10% stronger than in the FFF, although showing the same patterns. This effect, due to scattered light after the grating, has also been faced by Carter et al. (1986). In order to remove these two effects, we first separated through filtering, the interference fringe system from the flat-field higher and lower spatial frequencies. We emphasize the fact that, using at this stage a filtering procedure such as a median filter, avoids any spectral degradation to be applied to the SF. Then, on one side the "fringeless" FFF was used to correct the SF. On the other side, the frame containing only the fringe system was translated along the dispersion by the required shift and its intensity scaled so as to match the fringe system observed in the SF. This method proved to be quite powerful and allowed us to reduce fringe residuals in most of our spectra to a level comparable to the data noise (Fig. 1).

Because the near-infrared spectral range contains many atmospheric absorption bands (AAB), it is imperative to remove them carefully from star cluster and galactic spectra, by means of comparison with hot stars containing very few intrinsic absorption

**Table 2** (continued)

| | | | | | | | | | | | | |
|---|---|---|---|---|---|---|---|---|---|---|---|---|
| Sa I' | | | -22.3 < M < -22.0 | | | | | | | | | |
| 5064 | 1.3 | -2.3 | 24.9 | 6.4 | 6.8 | 2.2 | 9.1 | 4.1 | 2.6 | 5.4 | 4.3 | 1.9 |
| Sa II' | | | -21.9 < M < -21.0 | | | | | | | | | |
| 2811 | 1.2 | 0.4 | 26.8 | 8.5 | 9.9 | 2.3 | 13.7 | 4.5 | 3.2 | 6.0 | 4.9 | 4.0 |
| 3358 | 0.7 | -1.0 | 26.3 | 8.6 | 8.2 | 1.6 | 13.8 | 3.8 | 2.6 | 4.7 | 3.7 | 3.2 |
| 7049 | 1.2 | -1.2 | 30.7 | 6.9 | 7.8 | 2.0 | 14.4 | 4.2 | 2.7 | 5.5 | 4.3 | 3.6 |
| 4767 | 1.0 | 1.8 | 27.7 | 6.6 | 7.0 | 2.0 | 11.4 | 4.6 | 3.5 | 5.9 | 5.0 | 2.8 |
| 7079 | 1.2 | 2.1 | 24.4 | 8.7 | 8.9 | 1.6 | 11.5 | 4.1 | 2.9 | 5.1 | 4.0 | 2.6 |
| 5101 | 0.7 | -3.8 | 27.4 | 7.0 | 7.8 | 2.2 | 11.8 | 5.0 | 3.7 | 6.1 | 5.0 | 3.1 |
| Sa III' | | | -20.9 < M < -19.8 | | | | | | | | | |
| 6942 | 1.3 | -1.4 | 28.0 | 8.3 | 7.0 | 2.6 | 12.4 | 4.0 | 2.9 | 5.7 | 4.6 | 2.2 |
| 2781 | 1.4 | 0.5 | 25.0 | 6.4 | 7.9 | 1.8 | 11.7 | 4.8 | 3.3 | 5.6 | 4.4 | 2.3 |
| 4856 | 0.3 | -2.1 | 24.4 | 7.6 | 7.8 | 1.7 | 11.8 | 4.4 | 2.7 | 5.6 | 4.2 | 3.2 |
| 6684 | 0.4 | 2.1 | 24.4 | 7.8 | 7.9 | 1.5 | 12.5 | 4.7 | 3.3 | 6.5 | 5.3 | 2.9 |
| 5121 | 1.1 | 1.2 | 24.6 | 7.5 | 8.0 | 1.9 | 12.0 | 4.7 | 3.4 | 6.3 | 5.2 | 2.1 |
| Sb I' | | | -22.7 < M < -22.0 | | | | | | | | | |
| 3223 | 1.0 | 0.0 | 23.7 | 8.1 | 7.7 | 1.8 | 11.4 | 4.3 | 2.9 | 5.6 | 4.4 | 1.7 |
| 6782 | 0.0 | -6.9 | 22.1 | 5.8 | 8.1 | 2.9 | 11.8 | 3.1 | 1.8 | 4.1 | 2.9 | 1.7 |
| Sb II' | | | -21.9 < M < -21.0 | | | | | | | | | |
| 5612 | 0.3 | -1.7 | 21.9 | 6.6 | 7.4 | 1.4 | 12.3 | 4.4 | 3.1 | 4.6 | 3.6 | 1.8 |
| Sb III' | | | -20.9 < M < -20.3 | | | | | | | | | |
| 4462 | 1.6 | 0.7 | 27.0 | 9.8 | 8.6 | 1.7 | 17.6 | 5.0 | 2.7 | 6.4 | 4.6 | 3.2 |
| 3887 | 0.6 | -9.6 | 18.8 | 4.5 | 8.5 | 2.4 | 12.2 | 4.0 | 2.9 | 5.9 | 5.0 | 3.7 |
| Sc I' | | | -22.4 < M < -22.0 | | | | | | | | | |
| 6925 | 0.6 | -0.6 | 24.1 | 6.5 | 8.1 | 2.1 | 13.2 | 4.2 | 2.8 | 5.9 | 4.8 | 3.9 |
| 7329 | 1.6 | -0.8 | 27.0 | 6.3 | 7.0 | 1.9 | 11.2 | 3.4 | 2.3 | 5.0 | 4.1 | 2.6 |
| Sc II' | | | -21.9 < M < -21.0 | | | | | | | | | |
| 6744 | 0.5 | -1.1 | 24.9 | 8.2 | 7.1 | 1.4 | 11.7 | 4.3 | 3.3 | 6.5 | 5.6 | 2.6 |
| 6699 | 0.0 | -8.6 | 16.0 | 8.5 | 5.4 | 1.7 | 13.4 | 4.0 | 2.5 | 4.4 | 3.1 | 2.6 |
| 6923 | 0.6 | -2.0 | 23.2 | 6.5 | 7.9 | 1.6 | 14.7 | 4.3 | 2.6 | 6.0 | 4.6 | 4.5 |
| 3054 | 1.9 | 0.7 | 23.8 | 7.6 | 9.9 | 2.1 | 9.6 | 4.1 | 2.6 | 5.5 | 4.3 | 1.7 |
| 2997 | 0.7 | -45.0 | 22.3 | 9.1 | 9.2 | 1.2 | 14.9 | 4.4 | 3.2 | 5.9 | 4.9 | 2.4 |
| 2442 | 0.8 | -12.3 | 22.4 | 6.7 | 6.9 | 2.5 | 14.4 | 4.2 | 2.5 | 6.3 | 4.8 | 3.7 |
| 5236 | 0.4 | -78.0 | 20.8 | 7.8 | 5.5 | 1.2 | 14.0 | 4.7 | 3.1 | 5.4 | 4.1 | 1.6 |
| Sc III' | | | -20.9 < M < -20.9 | | | | | | | | | |
| 4981 | 1.6 | -13.1 | 22.4 | 8.7 | 7.2 | 3.5 | 15.9 | 4.9 | 3.0 | 6.1 | 4.4 | 4.1 |
| Seyferts | | | -21.3 < M < -21.2 | | | | | | | | | |
| 6300 | -0.4 | -14.0 | 18.8 | 6.6 | 7.3 | 2.6 | 12.5 | 4.5 | 3.3 | 6.7 | 5.8 | 2.1 |
| 5643 | -3.5 | -76.2 | 12.3 | 3.4 | 5.5 | 2.4 | 11.9 | 3.6 | 2.5 | 5.8 | 4.9 | 1.7 |
| Amorphous | | | M = -18.3 | | | | | | | | | |
| 5253 | 0 | -901 | -99 | -21 | 0 | 0 | 0 | 0 | 0 | 0 | 0 | -2 |

| | | | | | | | | |
|---|---|---|---|---|---|---|---|---|
| Sa I' | | | -22.3 < M < -22.0 | | | | | |
| 5064 | 4.4 | 3.8 | 1.8 | 8.3 | 0.94 | 0.95 | 0.95 | 0.91 | 0.91 | 0.90 | 0.89 |
| Sa II' | | | -21.9 < M < -21.0 | | | | | |
| 2811 | 4.9 | 4.1 | 2.2 | 7.8 | 0.95 | 0.93 | 0.95 | 0.92 | 0.91 | 0.91 | 0.91 |
| 3358 | 4.8 | 4.1 | 1.9 | 9.6 | 0.95 | 0.95 | 0.96 | 0.94 | 0.93 | 0.93 | 0.93 |
| 7049 | 4.8 | 3.8 | 2.3 | 7.8 | 1.03 | 1.06 | 1.08 | 1.07 | 1.06 | 1.06 | 1.04 |
| 4767 | 4.3 | 3.4 | 1.7 | 5.6 | 1.01 | 0.99 | 1.01 | 1.00 | 0.99 | 0.99 | 1.01 |
| 7079 | 4.3 | 3.3 | 1.2 | 12.8 | 1.02 | 1.00 | 1.03 | 0.99 | 0.98 | 0.98 | 0.99 |
| 5101 | 4.5 | 3.6 | 1.6 | 7.9 | 1.01 | 1.00 | 1.03 | 1.03 | 1.03 | 1.04 | 1.06 |
| Sa III' | | | -20.9 < M < -19.8 | | | | | |
| 6942 | 4.8 | 3.7 | 2.5 | 8.8 | 0.95 | 0.95 | 0.95 | 0.90 | 0.89 | 0.88 | 0.86 |
| 2781 | 4.1 | 3.3 | 2.2 | 8.2 | 0.96 | 0.97 | 0.98 | 0.94 | 0.93 | 0.93 | 0.91 |
| 4856 | 4.6 | 3.3 | 2.6 | 5.3 | 0.99 | 0.98 | 1.00 | 1.00 | 1.00 | 1.00 | 0.99 |
| 6684 | 5.0 | 3.9 | 1.7 | 7.9 | 0.92 | 0.90 | 0.92 | 0.89 | 0.89 | 0.88 | 0.87 |
| 5121 | 4.5 | 3.6 | 0.7 | 5.3 | 1.04 | 1.00 | 1.00 | 0.98 | 0.97 | 0.96 | 0.96 |
| Sb I' | | | -22.7 < M < -22.0 | | | | | |
| 3223 | 4.1 | 3.0 | 1.6 | 7.1 | 0.94 | 0.93 | 0.93 | 0.91 | 0.90 | 0.89 | 0.89 |
| 6782 | 5.0 | 3.8 | 3.3 | 7.9 | 0.97 | 0.97 | 0.97 | 0.95 | 0.95 | 0.95 | 0.95 |
| Sb II' | | | -21.9 < M < -21.0 | | | | | |
| 5612 | 3.8 | 3.4 | 1.3 | 16.5 | 0.96 | 0.94 | 0.91 | 0.87 | 0.85 | 0.84 | 0.84 |
| Sb III' | | | -20.9 < M < -20.3 | | | | | |
| 4462 | 4.7 | 3.2 | 2.1 | 10.8 | 0.96 | 0.96 | 0.97 | 0.95 | 0.94 | 0.94 | 0.94 |
| 3887 | 4.5 | 3.6 | 1.5 | 9.3 | 0.99 | 0.99 | 1.00 | 1.00 | 1.00 | 0.99 | 1.01 |
| Sc I' | | | -22.4 < M < -22.0 | | | | | |
| 6925 | 5.4 | 4.3 | 2.2 | 6.7 | 0.95 | 0.93 | 0.94 | 0.92 | 0.92 | 0.92 | 0.92 |
| 7329 | 4.7 | 4.0 | 3.0 | 9.8 | 0.99 | 0.99 | 0.99 | 0.95 | 0.93 | 0.92 | 0.91 |
| Sc II' | | | -21.9 < M < -21.0 | | | | | |
| 6744 | 4.5 | 3.9 | 1.4 | 10.7 | 1.00 | 0.99 | 1.00 | 0.98 | 0.97 | 0.97 | 0.96 |
| 6699 | 5.7 | 4.5 | 4.2 | 8.2 | 0.97 | 0.95 | 0.94 | 0.93 | 0.93 | 0.93 | 0.94 |
| 6923 | 6.3 | 5.1 | 2.8 | 7.3 | 0.96 | 0.95 | 0.96 | 0.95 | 0.96 | 0.96 | 0.97 |
| 3054 | 3.8 | 2.9 | 2.7 | 7.5 | 0.96 | 0.98 | 1.01 | 0.98 | 0.96 | 0.94 | 0.92 |
| 2997 | 5.4 | 4.5 | 1.0 | 10.4 | 0.96 | 0.97 | 0.97 | 0.94 | 0.94 | 0.93 | 0.93 |
| 2442 | 5.0 | 3.8 | 2.3 | 5.2 | 1.10 | 1.14 | 1.20 | 1.23 | 1.28 | 1.32 | 1.35 |
| 5236 | 5.4 | 4.3 | 1.8 | 4.9 | 0.84 | 0.79 | 0.72 | 0.66 | 0.64 | 0.63 | 0.61 |
| Sc III' | | | -20.9 < M < -20.9 | | | | | |
| 4981 | 4.8 | 3.2 | 3.3 | 2.3 | 1.07 | 1.08 | 1.08 | 1.09 | 1.10 | 1.11 | 1.11 |
| Seyferts | | | -21.3 < M < -21.2 | | | | | |
| 6300 | 4.8 | 4.3 | 1.6 | 6.9 | 0.97 | 0.96 | 0.95 | 0.92 | 0.91 | 0.91 | 0.92 |
| 5643 | 4.1 | 3.5 | 0.6 | -1.5 | 1.04 | 1.03 | 1.03 | 1.03 | 1.02 | 1.02 | 1.02 |
| Amorphous | | | M = -18.3 | | | | | |
| 5253 | -2 | 0 | -8 | -87 | 0.83 | 0.78 | 0.72 | 0.66 | 0.61 | 0.57 | 0.52 |

lines. For this purpose, we observed the standard stars LTT 3218, 6248, and 7987, which are hot white dwarfs usually considered for flux calibration in the near-infrared (Baldwin and Stone, 1984). The star LTT 6248 is somewhat cooler than the other two and exhibits detectable Ca II triplet which was straightforwardly removed. These three stars showing an H$\alpha$ absorption line, the corresponding spectral range was set to unity in the atmospheric correction files, owing to the absence of AAB around. We also verified that Paschen lines were negligible in the stellar spectra. Ideally, for each cluster or galactic nucleus, a hot star should be observed simultaneously and at the same airmass, if we wish to achieve a perfect AAB cancellation. In practice, we observed a standard star at the beginning, middle and end of each night. Comparison of the AAB strengths in these stars revealed that the atmospheric absorption remained stable within each of the 5 nights. We have displayed in Fig. 2 an example of the normalized atmospheric correction file derived from the three stars within a given night, as well as the spectra for one of the stars before and after this correction was applied. We also recall the main AAB in our spectral range. Standard stars were observed at small airmasses and so were most of the galaxies and Galactic star clusters. In contrast, LMC clusters were often observed at larger

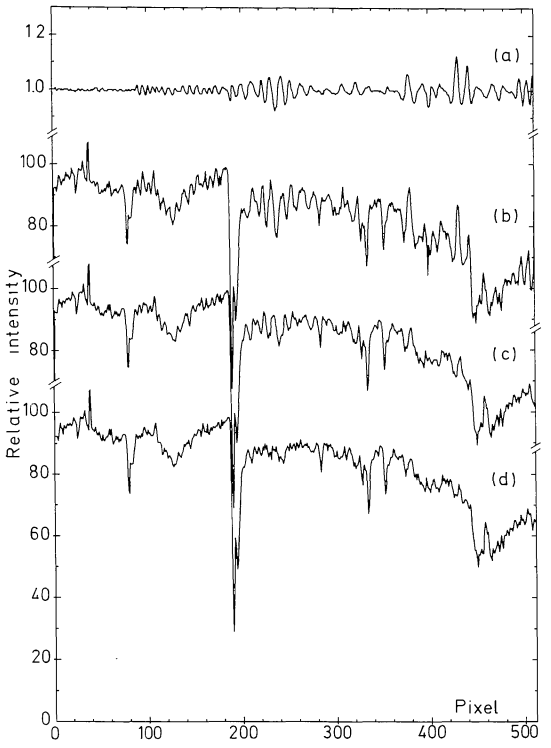


**Fig. 1.** The fringe correction, (a) the fringe system isolated from the flat field, (b) galaxy corrected by the fringeless flat field, (c) simple division of the spectrum in (b) by the fringe system in (a) showing that fringe residuals remain, (d) the spectrum in (b) divided by the fringe system (a) after shifting the latter by the required pixel number and matching the small fringe amplitude difference. The fringe residuals are then essentially indistinguishable from the noise

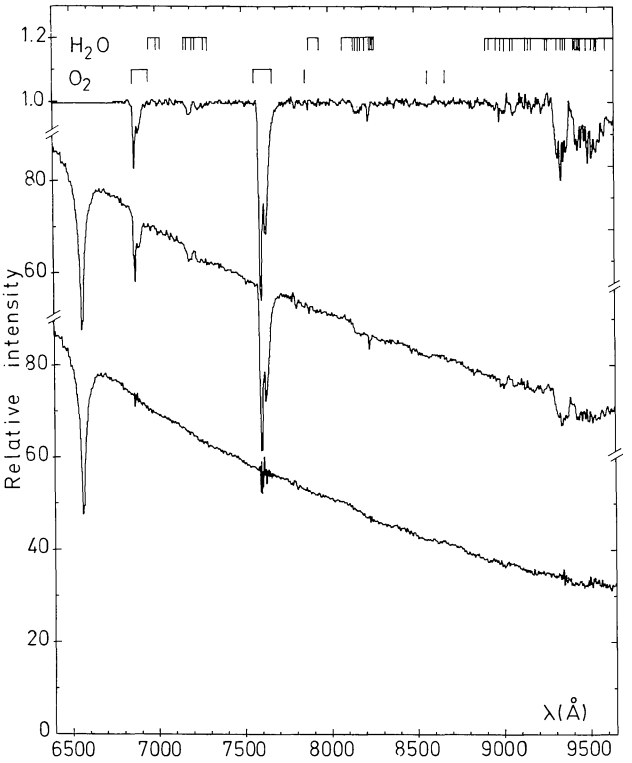


**Fig. 2.** The atmospheric correction, (a) correction file derived from 3 standard stars in one of the nights, (b) a standard star spectrum affected by atmospheric absorptions, (c) the corrected spectrum

airmasses, AM ~ 2. In order to cancel at best the stronger atmospheric absorptions seen at such large airmasses, we determined for each object a constant percentual level p% to be subtracted from the normalized atmospheric correction file, using the strongest $O_2$ and $H_2O$ AAB as a control for residuals. The simultaneous cancellation of molecular oxygen and water vapor absorption strengths indicates that they follow the same linear dependence on airmass for AM ≦ 2, described as p% = 20.3 (AM-1). The precision of atmospheric absorption corrections is estimated from the rms residuals measured in the corresponding windows for the hot standard stars. The strongest features, $O_2$ in windows No. 67 and No. 70A and $H_2O$ in No. 87 provide values of respectively 5%, 6%, and 12%. For weaker atmospheric features, residuals are difficult to estimate since they become smaller than the measurement precision. A precision level of 10% for the corrections, together with the mean value $W \sim 1.7$ Å for $H_2O$ contamination in the Na I 8190 Å window of hot standard stars indicate that the expected residuals for galaxies and clusters amount to 0.17 Å, thus are smaller than the 0.25 Å precision inferred for the measurements in this window.

## 3. Measurements

The star cluster spectra were corrected for Galactic reddening using the values compiled in Paper I. Galactic nuclei were corrected for (i) the Galactic reddening described by a cosecant law with absorption free polar caps and (ii) the intrinsic reddening due to inclined discs according to the template method described in Paper III and to the values given therein. Galactic nuclear spectra were then corrected for redshift with the velocities provided in Paper III. We confirm from our near-infrared data that NGC 6942 has a velocity $V = 3200\ \mathrm{km\,s^{-1}}$ as derived previously (Paper III), the value in Sandage and Tammann (1981) being incorrect. The fully corrected continuum points, expressed in $F_\lambda$ units and normalized to that at 5870 Å by means of the overlapping region for each spectrum are presented in Tables 1 and 2, respectively for star clusters and galaxies. In all figures in this study, the continuum distribution corresponds to reddening corrected spectra.

In view of defining windows for $W$ measurements of well-known features, and of providing identifications for weaker ones, we generated high signal to noise mean spectra for typical red strong-lined and blue populations. These are shown in Fig. 3a and b respectively. The red spectrum is a mean of 22 redshift corrected early type galaxies which are free from emission lines. The fact that the originally observed spectra correspond to different galaxy velocities ensures that all rest frame sources of uncertainties, namely residuals from night sky emission, atmospheric absorption and fringes, average out and thus every weak feature in Fig. 3a is real. This may not be the case in Fig. 3b where the blue spectrum consists of a mixture of young LMC clusters, the Galactic open cluster NGC 6705 and the blue lenticular NGC 5102. However, the Paschen series is clearly seen up to P18. We provide

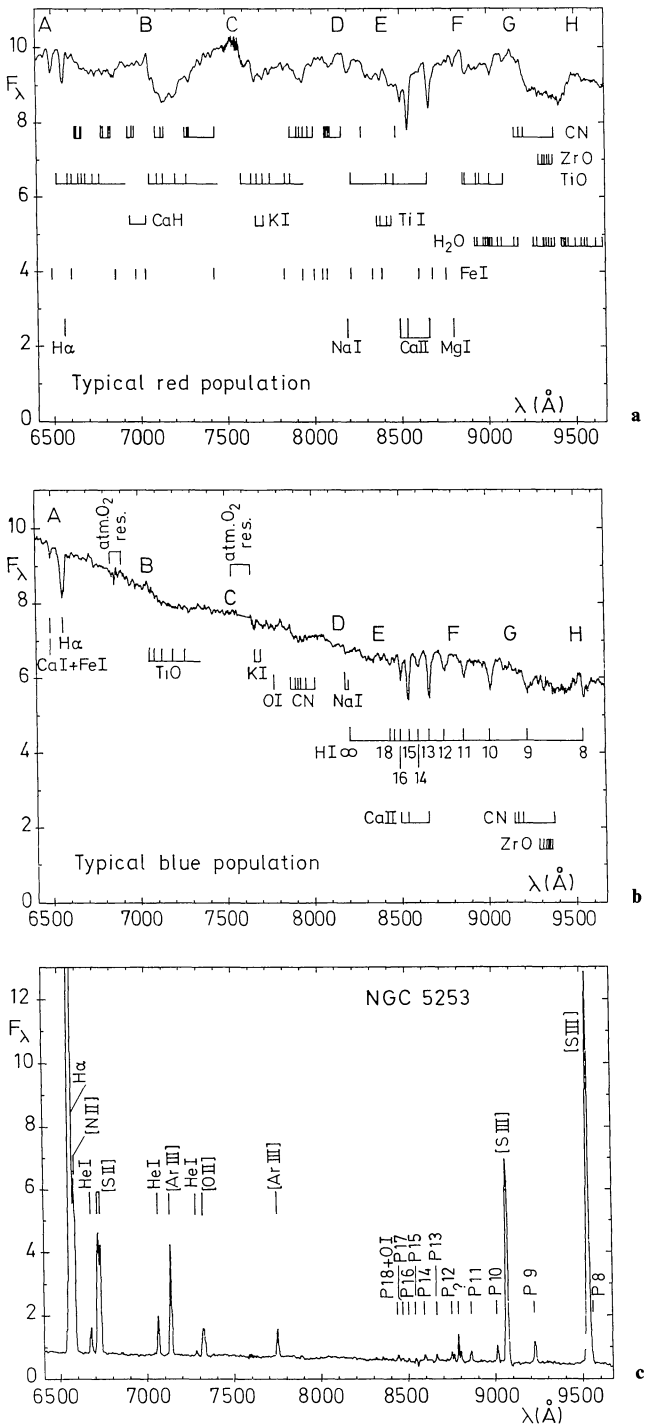


**Fig. 3a–c.** High signal-to-noise spectra for feature identifications, **a** mean of 22 red strong-lined early type galaxies, **b** typical blue population built up from Magellanic Cloud and Galactic blue clusters, as well as from the blue S0 galaxy NGC 5102, **c** the emission line galaxy NGC 5253

in Fig. 3c one example of an emission line galaxy (NGC 5253) in order to show which windows might be seriously affected by emission in such objects.

The parameters of and main contributors to the absorption line windows are listed in Table 3. These windows have been defined from the star cluster sample and are a continuation of the listing initiated in the visible range (Paper I). In Fig. 3a, we have shown the adopted criteria for continuum tracings. Points A, C, F, and G are very possibly true continuum points. Points B and D are certainly depressed by molecular and/or line absorption but still represent local maxima and were selected in order not to rely on a few points only. Measurements of the strong absorption CN, ZrO from 9130 to 9490 Å, are unfortunately very dependent on point H which is affected by molecular absorption and furthermore is subject to border effects in some of the spectra. Thus we do not use this feature. We provide in Tables 1 and 2 the equivalent widths $W$ for a selection of 13 features. Line EF matches an alternative tracing which is intended to minimize molecular absorption in the Ca II infrared triplet windows. It corresponds to the local continuum defined for stellar spectra by Jones et al. (1984). Point E departs from the DF line more particularly in the case of strong-lined galaxies and very metal rich globular clusters. Whenever differences arise between the feature equivalent widths outlined by the two different tracings, we provide in Tables 1 and 2 the two corresponding values. Line identifications and continuum points displayed in Fig. 3a are most important for the selection of spectral ranges in future analysis of high dispersion spectra. Absorptions being present almost everywhere in the near-infrared, some doubt raises about the usual definition of molecular band indices with respect to flux side bands. Indeed absorptions may quite often be very important in the so-called continuum side bands, changing the desired strength measurement of a feature into that of a ratio between two features. In particular, such indices may hide important metallicity dependences.

In order to test the consistency of our IDS and CCD data sets, we have compared the results obtained for a window in the overlapping region, Hα (Fig. 4). This demonstrates that the measurements from the two data sets are in good agreement, whether Hα appears in absorption or in emission and this conclusion holds true for more than 3 decades.

In the case of star cluster spectra, a further check should be made about the consistency of the spatial coverage for any cluster belonging to the two data sets. To achieve this, the use of a molecular band is more appropriate than that of Hα, since molecular absorptions are quite strong in bright giant stars and hence would reveal any sensible difference in the spatial sampling. However, the strong TiO λλ 7050, 7464 in the overlapping region could not be used in the case of the IDS data set, because the spectra were not corrected for atmospheric absorption. We decided to use instead the same molecule TiO, seen in its λλ 6156, 6386 band with the IDS and in its λλ 7050, 7464 band with the CCD, these two bands being expected to vary together in first order (Fig. 5). The scatter observed for star clusters is not larger than that for galactic nuclei which certainly are not subject to any sampling effect. In conclusion, we are fairly confident that using two different devices, IDS and CCD, did not affect much the homogeneity of our data set.

## 4. Star cluster properties as a function of age and metallicity

The main properties of star cluster spectra in the near-infrared can be seen in Fig. 6a and b which present respectively a metallicity sequence for Galactic Globular Clusters (GGC) and an age sequence for young and intermediate age Magellanic Cloud Clusters (MCC). Two major conclusions arise from these figures: (i) the strength of molecular bands increases drastically in metal rich GGC, and (ii), in the MCC age sequence, a continuum slope

**Table 3.** Definition of the windows from the star cluster sample

| Window | $\Delta\lambda$ (Å) | $\bar{W}/\Delta\lambda$ [1] | Absorbers |
|---|---|---|---|
| No. 59 | 6474–6540 | 0.01 | Ca I; Fe I; Ba II; CN; l.c.m. [2] |
| 60 | 6540–6586 | 0.06 | H$\alpha$; TiO; Fe I |
| 61 | 6586–6670 | 0.01 | TiO; Fe I; CN |
| 62 | 6670–6736 | 0.02 | TiO; Ca I; Fe I |
| 63 | 6736–6858 | 0.02 | TiO; CN; Fe I; CaH |
| 64 | 6858–6934 | 0.01 | Atm $O_2$ res.; CN; CaH |
| 65 | 6934–7050 | 0.01 | CaH; CN; Fe I; l.c.m. |
| 66 | 7050–7158 | | TiO; CN; Ca I; Fe I; He I; Ni I |
| 67 | 7158–7274 | 0.03 | TiO; Atm. $H_2O$ res. |
| 68 | 7274–7464 | | TiO; CN; Fe I; VO |
| 69 | 7464–7580 | 0.00 | CaH; Fe I; l.c.m. |
| 70A | 7580–7640 | −0.01 | Atm. $O_2$ res.; TiO; l.c.m. |
| 70B | 7640–7704 | 0.03 | TiO; K I; Atm. $O_2$ res. |
| 71 | 7704–7852 | 0.02 | TiO; Fe I; O I |
| 72 | 7852–8040 | 0.02 | CN; VO; Fe I |
| 73 | 8040–8160 | 0.01 | CN; Fe I; l.c.m. |
| 74 | 8160–8234 | 0.02 | Na I; Fe I; TiO; H I; Atm $H_2O$ res. |
| 75 | 8234–8408 | 0.03 | TiO; Ti I; Fe I; CN; H I |
| 76 | 8408–8476 | | TiO; Ti I; H I(P17, 18) |
| 77 | 8476–8520 | 0.05 | Ca II; TiO; H I(P16); Fe I; CN |
| 78 | 8520–8564 | 0.09 | Ca II; TiO; H I(P15); VO |
| 79 | 8564–8640 | 0.02 | TiO; H I(P14); VO |
| 80 | 8640–8700 | 0.07 | Ca II; H I(P13); TiO; VO; Fe I |
| 81 | 8700–8786 | 0.02 | H I(P12); Fe I; CN; ZrO |
| 82 | 8786–8844 | 0.01 | Mg I; Fe I; l.c.m. |
| 83 | 8844–8940 | 0.03 | H I(P11); TiO |
| 84 | 8940–9066 | | H I(P12); TiO; Fe I |
| 85 | 9066–9130 | 0.03 | TiO; l.c.m. |
| 86 | 9130–9270 | 0.03 | CN; H I(P9) |
| 87 | 9270–9490 | 0.05 | ZrO; $H_2O$ [3]; CN; Atm. $H_2O$ res |
| 88 | 9490–9600 | 0.02 | H I(P8); $H_2O$; Atm. $H_2O$ res; l.c.m |

*Notes to Table 3*:
[1] $\bar{W}/\Delta\lambda$ for metallic features appears to be systematically lower than in the study of the visible data refering to a larger sample. Although the present infrared cluster sample still covers the entire metallicity range specified in Paper I, as a mean the clusters selected for the infrared study have a lower metal content and this explains the lowering of $\bar{W}/\Delta\lambda$
[2] l.c.m. = local continuum maximum
[3] We estimate that in this window, intrinsic $H_2O$ absorption may contribute significantly since other $H_2O$ bands are detected at longer wavelengths in stars and galaxies (Aaronson et al., 1978)

effect due to the blue stellar content is still detectable in the near-infrared range, as also revealed by the presence of the Paschen series in these spectra. However, this spectral range is obviously very sensitive to the flux contribution from low temperature stars. This can be seen more particularly at some short phases in the evolution of a young star cluster, when an accumulation of red evolved stars occurs, e.g. red supergiants at $t \sim 10^7$ yr (NGC 2004) and asymptotic giant branch (AGB) stars with massive progenitors at $t \sim 10^8$ yr (NGC 1866). The reality of the latter case, where AGB stars are expected to contribute significantly to the integrated flux for a short period of time in a blue cluster, is predicted theoretically (Renzini and Buzzoni, 1985; Chiosi et al., 1985) and is observed in the LMC cluster NGC 1866 besides evidences that the same effect is present in some Galactic open clusters (Paper I).

In the following analysis we adopt for NGC 1866 a value $[Z/Z_\odot] = -0.5 \pm 0.4$. The metallicity value $[Z/Z_\odot] = -1.2$ from Richtler and Nelles (1983) which was used in Paper I, is not compatible with the strong TiO bands observed in the present spectrum, nor with the metallicity expected for a blue LMC cluster under the chemical evolution scenario of the LMC, even if one takes into account the intrinsic metallicity dispersion observed for H II regions and red clusters (Bica et al., 1986). Also, Becker and Mathews (1983) deduced an almost solar metallicity by means of synthetic HR diagram fitting in this cluster.

We show in Figs. 7a, 7b and 7c respectively, the behaviour of metallic lines $W$(Na I 8190 Å), $W$(Ca II 8542 Å), and $W$(Ca II 8662 Å) as a function of metallicity. The relations are essentially single-valued, regardless the cluster age. Such a behaviour was expected from the trend already observed in the visible range

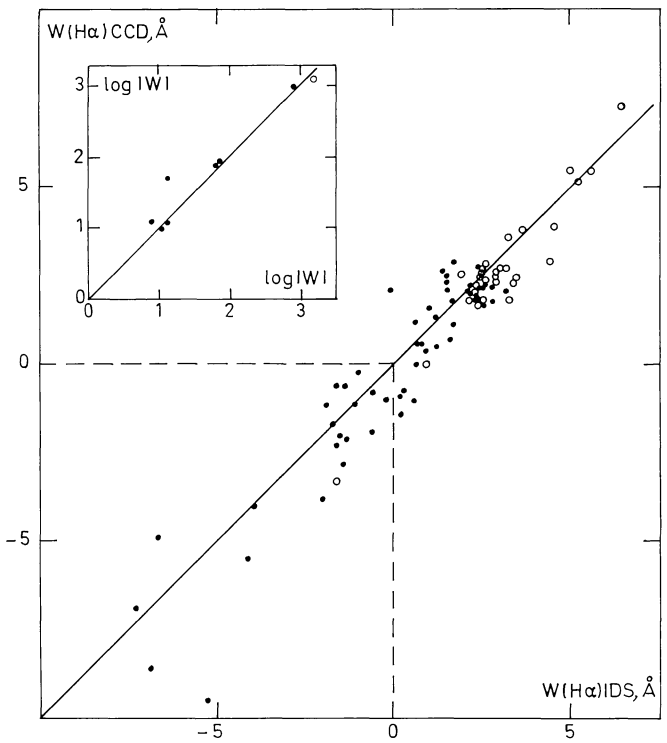


**Fig. 4.** Comparison of $W$(Hα) measurements derived from the IDS (abscissa) and CCD (ordinate) data sets. Open circles represent star clusters and H II regions, and black dots galactic nuclei. Negative values of $W$ correspond to an Hα line in emission and the very large emission lines are shown in a log-log inset in the upper left corner of the diagram

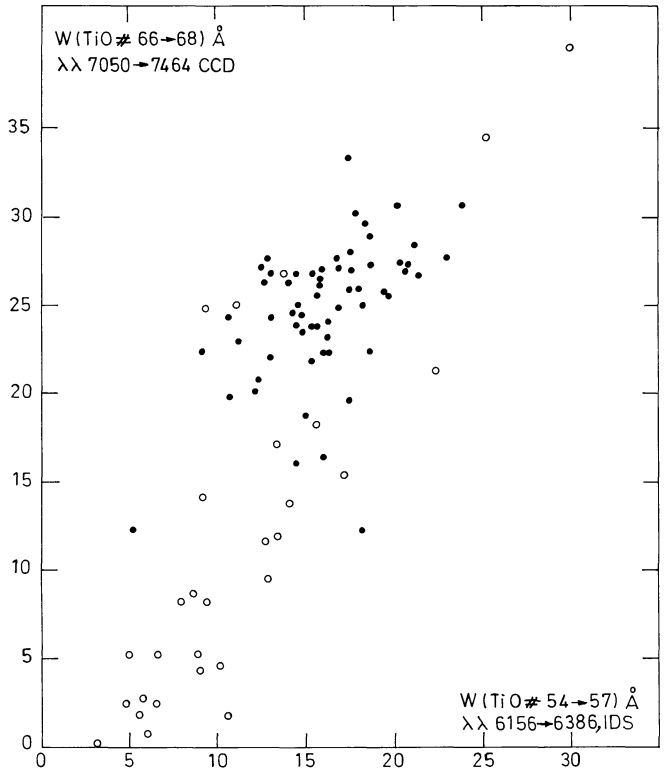


**Fig. 5.** Comparison of the strengths of two TiO bands showing that the observed scatter for star clusters (circles) is not larger than that for galactic nuclei (dots). This indicates that no major difference occured in the spatial coverage of the clusters, between the IDS and CCD observations

(Paper I) where isochrones in the $W$ vs $Z$ plane tended to merge at longer wavelengths, as a result of a decreasing dilution effect from the blue main sequence stars. Sources of scatter in Figs. 7a through 7c are various. In the Na I window the errors are relatively larger owing to the weakness of this feature. In the Ca II windows, contamination by TiO and Paschen lines are rather to be incriminated: TiO may reinforce the metallicity dependence while Paschen lines introduce a systematic increase for blue clusters whatever their metallicity is. TiO contamination is most important in the Ca II 8542 Å window and the Paschen absorption will affect more the Ca II 8662 Å window.

In first order, the windows dominated by molecular absorption share the same characteristic, e.g. TiO λλ 7050, 7464 for which the mean $W$ value increases steadily with $Z$ (Fig. 8a). But the scatter of points is larger than that observed for windows related to metal atomic lines. A comparison with Fig. 5 also demonstrates that the scatter is larger than that expected from observational errors and it is thus intrinsic. In particular it arises mostly from blue clusters rich in red evolved stars like NGC 2004 and NGC 1866. These clusters have stronger TiO bands than GGC of comparable metallicity, while other young clusters which are deficient in this red evolved population tend to show weaker TiO than GGC.

The reason why, in integrated spectra, molecular bands behave with $Z$ in a more complex way than atomic metal lines do, is certainly related to the fact that atomic lines can be formed throughout a wide range of stellar temperatures from early M up to F types which constitute the bulk of the flux emission from 6000 to 10 000 Å for clusters of all ages. On the other hand, molecular bands arise essentially from cool stars, and the flux contribution from these cool stars to the integrated light of a cluster strongly depends on the cluster age. Thus, as shown in Fig. 8b, abrupt changes in the equivalent width of molecular bands occur at the red supergiant ($t \sim 10^7$ yr) and at the AGB ($t \sim 10^8$ yr) phases. These rapid red phases are accompanied by a flattening of the near-infrared continuum slope as displayed in Fig. 8c (see also Fig. 6b). The behaviour of molecular bands also differs from that of atomic lines in the sense that they preferentially exhibit a non-linear dependence on $Z$. This effect is present in the CN and TiO windows (e.g. Fig. 8a), particularly for the GGC sample where age effects are absent: for $[Z/Z_\odot] < -1.0$ molecular absorptions are almost null while they become prominent at a metallicity around solar. On the contrary, metal atomic lines (e.g. Fig. 7a) exhibit a steady regular increase with $Z$. The increase rate may, however, change from one line to the other. Taking as a reference the $W$ value at $[Z/Z_\odot] = -1.0$, for an increase in metallicity by a factor 10, $W$(Na I λ 8190) increases by around 66%, $W$(Ca II λ 8542 + TiO) by 62% and $W$(Ca II λ 8542), corrected for TiO, by 55% (column 12 in Table 1). An intermediate behaviour between metallic lines and molecular bands is observed for windows in which both kinds of absorptions contribute equally. This can be seen in Fig. 9a and b the first one corresponding to windows

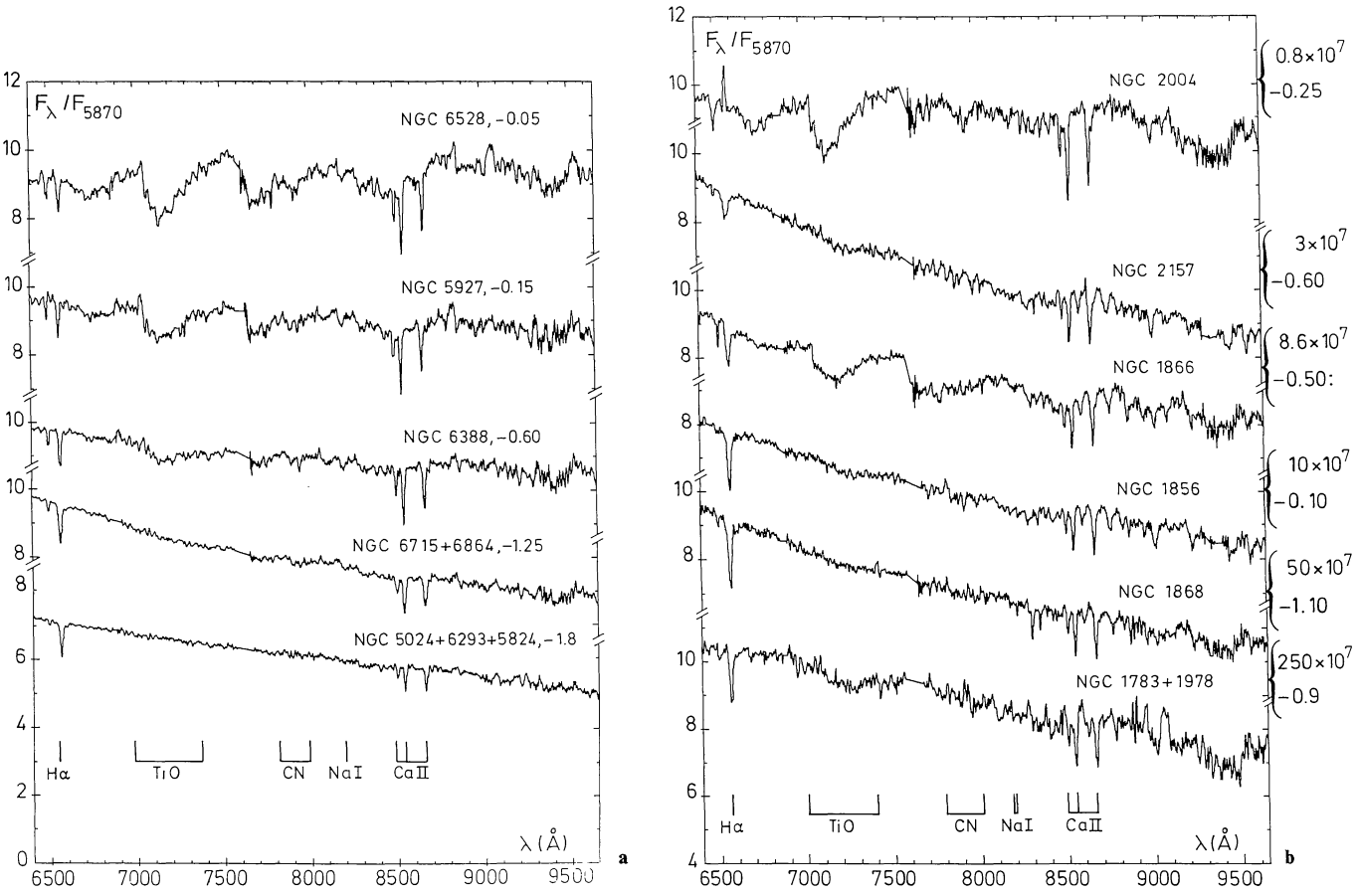


**Fig. 6.** **a** Downward metallicity sequence for Galactic globular clusters showing the increase of Ca II, Na I and molecular bands with $[Z/Z_{\odot}]$, **b** Age sequence for young clusters; the age and metallicity are provided in the right part of the figure. Ages around $10^7$ yr and $10^8$ yr are dominated by red evolved stars, as traced out by strong TiO molecular bands

Nos. 75 + 76 where the TiO absorption is significantly enhanced by Ti I and Fe I lines, and the second one corresponding to the smallest Ca II triplet line which is blend with a strong TiO molecular absorption.

Finally, we have displayed in Figs. 10a and 10b, the joined windows Nos. 83 + 84 which, in red clusters correspond to TiO absorption and in blue clusters are dominated by Paschen lines P10 and P11. In this case we face metallicity (Fig. 10a) and age (Fig. 10b) effects of comparable importance. Regarding the Ca II triplet, indeed weak Paschen lines may contribute to the window; but then, the metallic feature remains predominant even in blue clusters where, from the intensities of P17, P14, and P12 (Fig. 3a), we estimate that P16, P15, and P13 correspond to 45%, 36% and 45% of the absorption respectively in the Ca II $\lambda$ 8498, $\lambda$ 8542, and $\lambda$ 8662 windows.

As in Paper I, we present on the right part of Figs. 7 through 10, the corresponding histograms for spheroidal (E, S0) and spiral (Sa, Sb, Sc) galaxies. Such a comparison is necessary in view of population synthesis to be performed and presented in a forthcoming paper. In the near-infrared very metal rich globular clusters like NGC 6440 and 6528 exhibit metallic features comparable to the strongest-lined galaxies. For example NGC 6528 presents molecular bands even stronger than in any galaxy (compare Figs. 6a and 11, also). In the visible range (Paper I) these two clusters, together with NGC 6553, also showed $W$ for metallic features comparable to those observed in the strongest-lined galactic nuclei, with the exception of windows corresponding to Mg I + MgH and its surrounding. At that time, we adopted thus the conservative conclusion that 50% of the luminous galaxies could be described by the cluster library without any extrapolation in the $W$ vs metallicity plane. The spectra of galaxies should not necessarily be identical to those of very metal-rich globular clusters since the latter are expected to be single generation objects while galactic nuclei might cover a certain range in metallicity and age. However, systematic differences in the mean metallicity or age do not explain why some metallic features are slightly stronger and others slightly weaker among different objects. Several explanations could be raised, such as abundance anomalies for a few elements, line saturation effects or differences in the initial mass function (IMF). Another interpretation could simply be variations in the number of luminous stars in which particular features are strong. Globular clusters are star-rich but the number of luminous stars they contain is finite and subject to fluctuations. Thus, the near-infrared molecular band excess in NGC 6528 with respect to galaxies and to the otherwise similar globular cluster NGC 6440, could result from a slightly enhanced population of

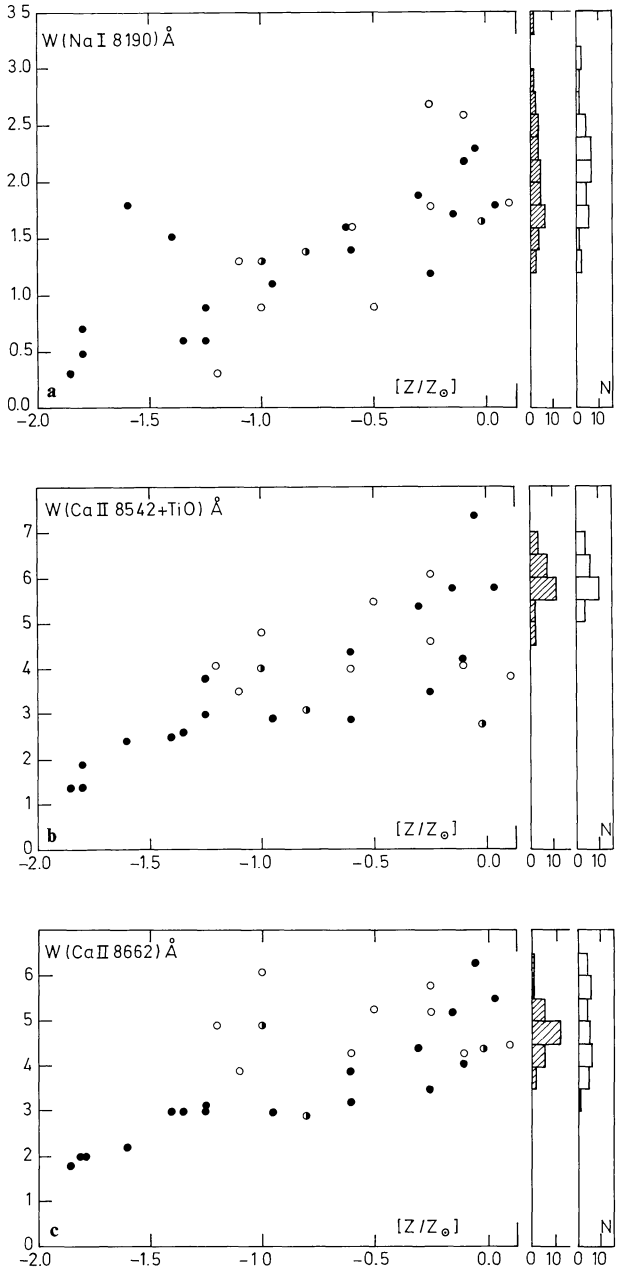


**Fig. 7a–c.** Metallic line windows as a function of metallicity. Filled circles are Galactic globular clusters, semi-empty and empty circles represent respectively intermediate age and young clusters. The relations are age-independent. On the right side we show histograms for spiral galaxies (hatched) and E + S0 galaxies respectively

bright M giant stars in which those features are very strong. Conversely, the weaker Mg I + MgH absorption in very metal rich globular clusters with respect to galaxies might be assigned to an excess, in the former, of K giants where this feature is weaker than in dwarfs (Spinrad, 1962). For the future population synthesis, it is thus, important to minimize fluctuation effects in the star cluster library, by interpolating the mean properties as a function of metallicity and age. Criteria for the interpolations were established in Paper I. The grid predictions for the near-infrared

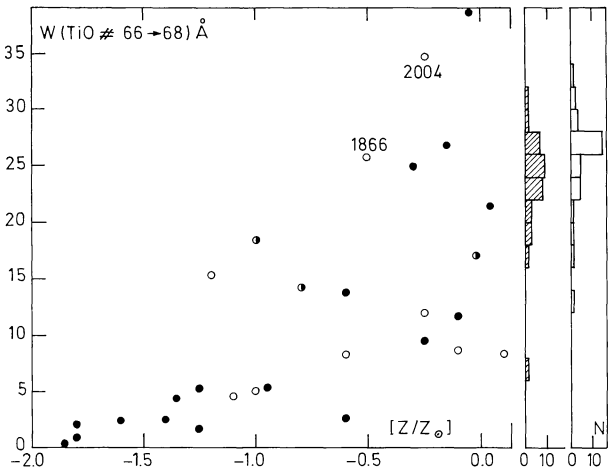


**Fig. 8a.** Behaviour of a strong molecular band as a function of metallicity; same symbols as in Fig. 7; for large metal content, some young clusters tend to lie below the globular clusters, of equal metallicity, while others (labelled) containing luminous red stars, tend to lie above.

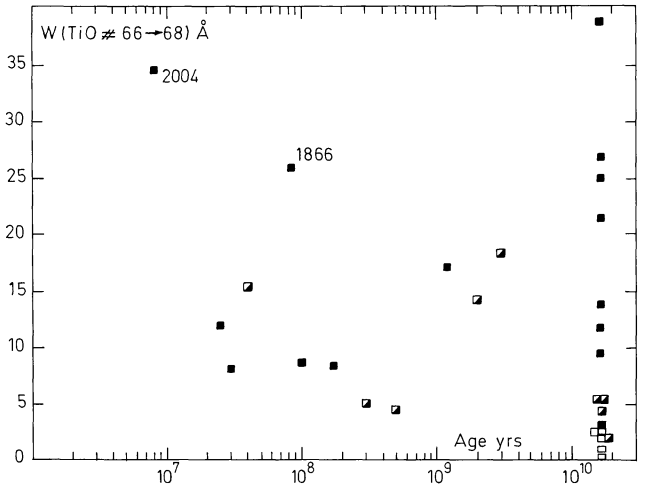


**Fig. 8b.** The same molecular band as a function of age. Young clusters in the red phases ($10^7$ and $10^8$ yr old) show prominent molecular absorption. Filled squares correspond to $[Z/Z_\odot] > -0.7$ semi-empty ones to $-1.4 < [Z/Z_\odot] < -0.7$ and empty ones to $[Z/Z_\odot] < -1.4$

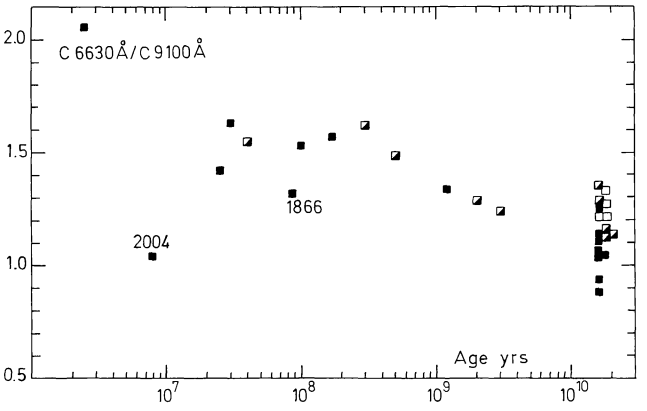


**Fig. 8c.** The near-infrared continuum slope as a function of age. Symbols as in Fig. 8b. Young clusters in the red phases have a flatter continuum than other young clusters. For comparison, we also show the H II region NGC 1714 in the upper left corner

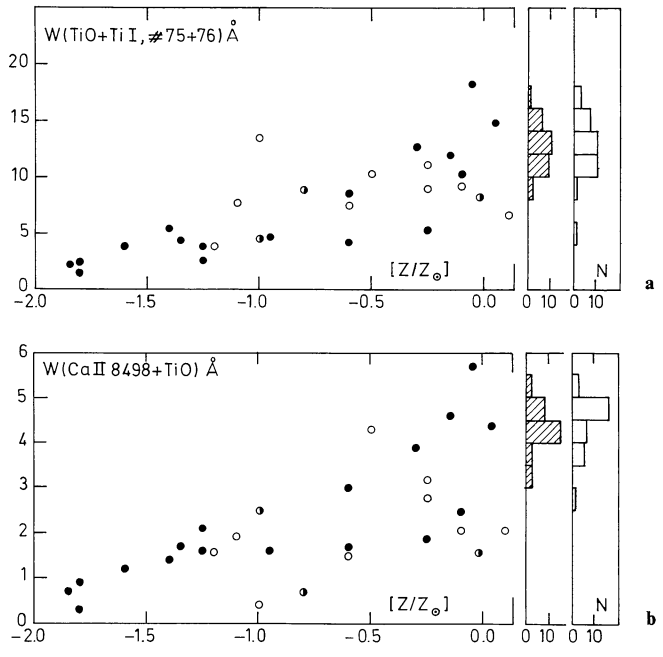


**Fig. 9a and b.** Windows in which molecular bands and metallic lines contribute with a comparable weight to the total absorption; their behaviour with Z is intermediate between those in Figs. 7 and 8a. Same symbols as in Fig. 7

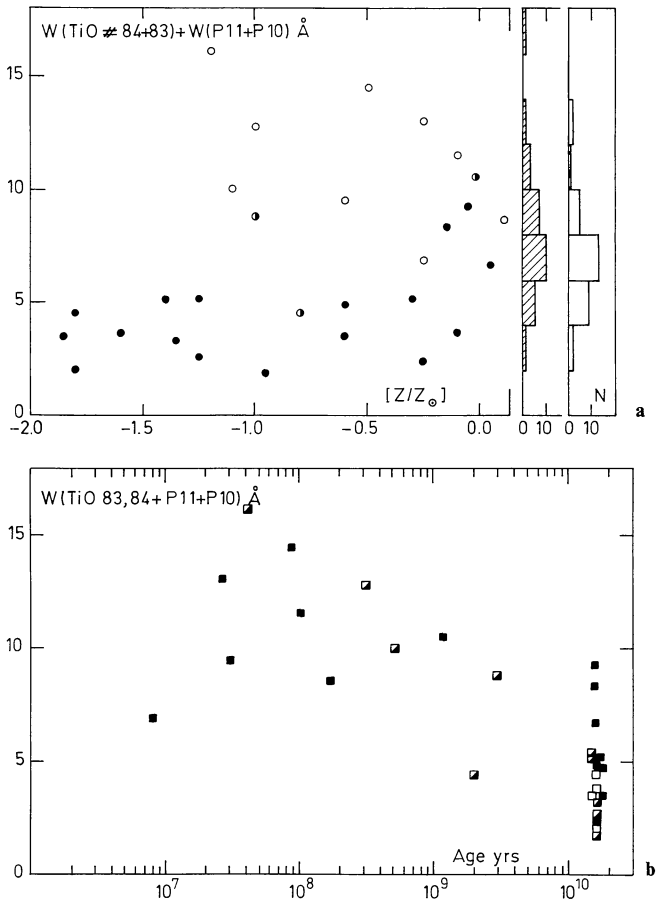


**Fig. 10a and b.** Behaviour with metallicity **a** and age **b** of a window dominated by molecular absorption in old clusters and Paschen lines in young ones. Symbols are respectively as in Figs. 7 and 8b

range are given in Appendix A, following the same format as that initially used for its visible counterpart (Paper II).

Early spectroscopic studies had included the very metal rich GGC NGC 6440, 6528 and 6553. In particular, Morgan (1960) pointed out the similarity of their spectrum with that of the nucleus in M31. Unfortunately, recent works comparing GGC to galaxy nuclei used, as metal rich clusters, NGC 6637 (M69) and NGC 6356 which are not as suitable (e.g. Faber, 1973; Aaronson et al., 1978; Frogel et al., 1978; Burstein et al., 1984). The integrated spectra and colours of the latter clusters are indeed like those of NGC 6388 (Fig. 6a) and thus, weak-lined with respect to massive galaxy nuclear spectra. Consequently, a consensus was established suggesting that GGC were not useful for population comparisons with galaxy nuclei, unless large extrapolations in metallicity were made for the cluster properties. This extrapolation problem was further exacerbated by the different metallicity scales proposed in the last 10 years based on 47 Tuc (NGC 104) and M71 (NGC 6838): different techniques led to metallicities ranging from solar to $[Z/Z_\odot] = -1.2$. Integrated properties of 47 Tuc and M71 are also similar to those of NGC 6388, and hence their spectrum is weak-lined with respect to those observed in massive galaxy nuclei. Presently, the best $[Z/Z_\odot]$ values for 47 Tuc and M71 range from $-0.6$ to $-0.8$ (Zinn and West, 1984; Gratton et al., 1986) and the metallicities we adopted in Paper I are from a calibration where 47 Tuc has $[Z/Z_\odot] = -0.7$. The cluster NGC 5927 (Fig. 6a) is 0.6 dex more metal-rich than 47 Tuc, on the basis of spectroscopic analysis of red giants (Cohen, 1983). However, values for the metal content in NGC 6440, 6528, and 6553 still rely on extrapolations and it would be interesting to derive them directly from individual member stars. Inspection of the integrated spectrum of NGC 6528 (Fig. 6a) and its locus in Figs. 7 and 8a, suggest that a value $[Z/Z_\odot]$ as large as $+0.3$ might be possible. Nevertheless we emphasize the fact that the GGC vs galaxy nuclei problem is solved by the present observations and those presented in Papers I and II: *the spectra of very strong-lined GGC are comparable to those of massive galaxies*, whatever their precise metallicity value. We also point out that the synthesis approach we have undertaken is little dependent on the adopted age and metallicity calibrations for the clusters. It relies rather upon the properties observed directly on the cluster spectra.

## 5. Spectral properties of galactic nuclei in the near-infrared

We have displayed in Fig. 11 examples of galactic spectra for different morphological type, luminosity groups. The spectra look similar, whatever the group, dominated by strong metallic features. Even extreme cases in the visible range like the blue objects NGC 5102 and 5236 do not show spectra much different than for the rest of the galaxy sample in this range. However it should be noticed that in the near-infrared we are not necessarily looking at the underlying old population of these two blue nuclei. Indeed we observe that the near-infrared flux in young star clusters is always a significant fraction of the visible one (Table 1). The burst of star formation 4 $10^8$ yr old in NGC 5102 (Paper III) and responsible for 70% of the light at 5870 Å, still dominates at 9100 Å with a 57% contribution. Information about the burst duration can also be derived as follows. The deep Hα absorption in the star clusters NGC 1831 and 1868 (Fig. 6b and Table 1) which have the same age as the burst in NGC 5102 (Paper III), indicates that Hα is just filled in by emission in the latter. This evidence, together with weak [N II] and [S II] line emission (Fig. 11) indicate that we are still observing a residual star formation

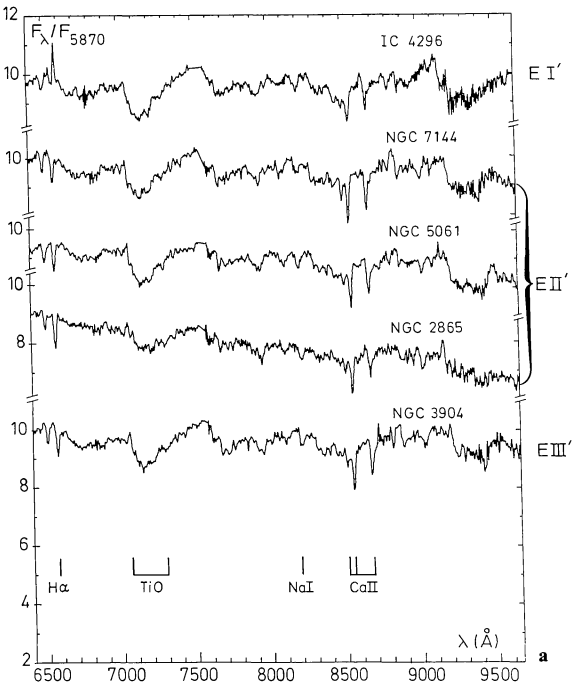


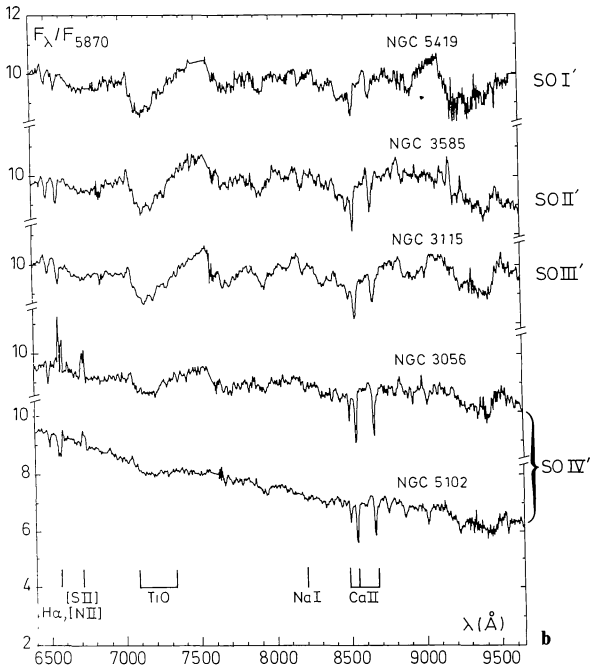


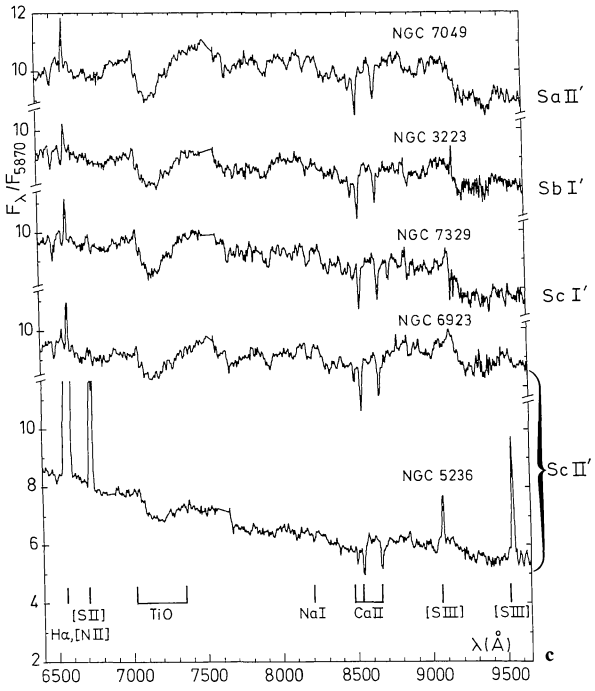


**Fig. 11a–c.** Examples of spectra of galactic nuclei for elliptical **a**, lenticular **b** and spiral **c** galaxies. Luminosity classes I′, II′, III′, and IV′ are according to Table 2 and were defined in Paper III

related to the strong burst initiated 4 $10^8$ yr ago. A detailed synthesis will possibly give more information about how the burst behaved in the meantime. The emission line spectrum of NGC 5236 originates at least in part, from H II regions. The continuum distribution as well as the Balmer lines higher than H$\delta$ which appear in absorption (Paper III) suggest that star formation has been taking place for several $10^7$ yr. Thus, some contribution to the strong molecular bands in the near-infrared necessarily originates from red supergiants $10^7$ yr old like in the star cluster NGC 2004 (Fig. 6b) or from the red stars at $10^8$ yr like in the cluster NGC 1866 if the burst extends further back in time. Other galaxies in Fig. 11, when examined in detail, present small systematic differences with respect to a mean spectrum. The elliptical galaxy NGC 2865 which contains a moderately old burst ($10^9$ yr, Paper III) still exhibits a detectable steeper continuum in the near-infrared. On the other hand, NGC 5061 which has a visible spectrum intermediate between that of NGC 2865 and the mean one for the rest of the group, is in the near-infrared indistinguishable from the other objects in its group. Finally, the lenticular galaxy NGC 3056 shows evidence of some metal deficiency with respect to more luminous groups.

We provide in Fig. 12a and b examples of the behaviour of $W$ with morphological type for a molecular band and for a metallic line. The $W$ values are quite comparable for the different morphological types. As our sample consists essentially of luminous galaxies ($M_B < -20$), this indicates that elliptical, lenticular and spiral galaxies cover a similar range of metallicities in their central regions. Just like in the visible spectra, molecular bands display a larger dynamical range of $W$ values than metallic lines do. This reflects a better sensitivity of molecular bands to metallicity, according to star cluster results (Sect. 4). Indeed, the mean metallicity of a massive galaxy is expected to fall in the range where molecular bands grow non-linearly with $Z$ (Sect. 4). The larger dynamical range of molecular bands can also be seen in Figs. 13a and 13b where we have plotted respectively $W$(TiO $\lambda\lambda$ 7050, 7464) vs $W$(CN $\lambda\lambda$ 7852, 8040), and $W$(Na I $\lambda$ 8190) vs $W$(Ca II $\lambda$ 8542).

In Figs. 14a and 14b, the behaviour of $W$(Ca II $\lambda$ 8542) and $W$(TiO $\lambda\lambda$ 7050, 7464) as a function of absolute magnitude $M_B$ of the galaxy, is demonstrated. No dependence of the Ca II triplet line with luminosity is observed, possibly a result of the smaller

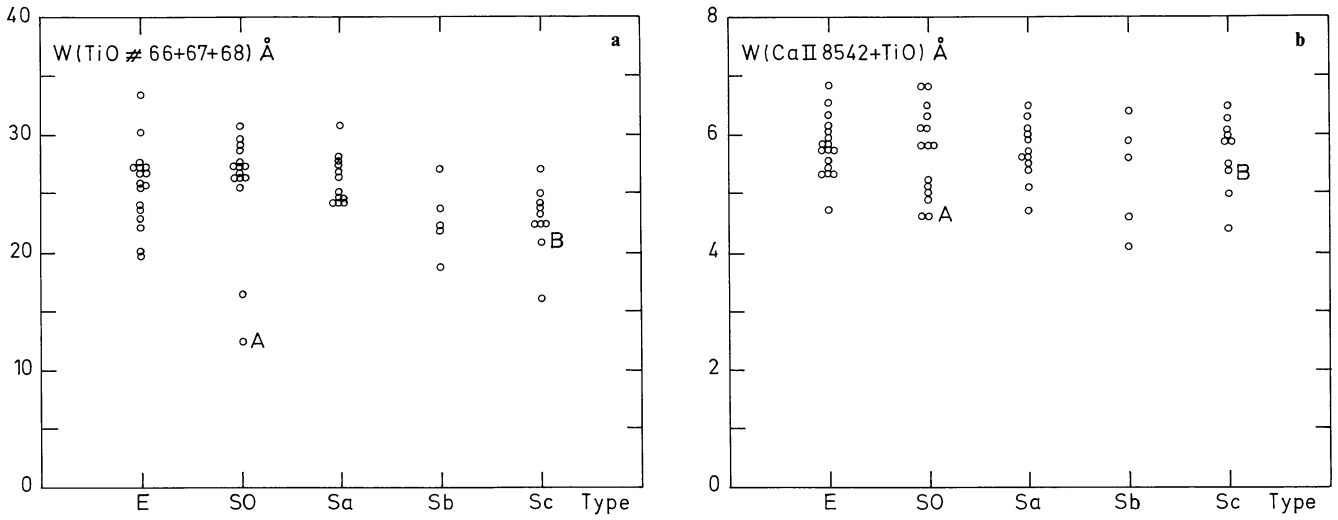


**Fig. 12a and b.** Behaviour of a molecular band **a**, a metallic line **b**, with different morphological types. Points labelled A and B correspond respectively to the blue galaxies NGC 5102 and 5236

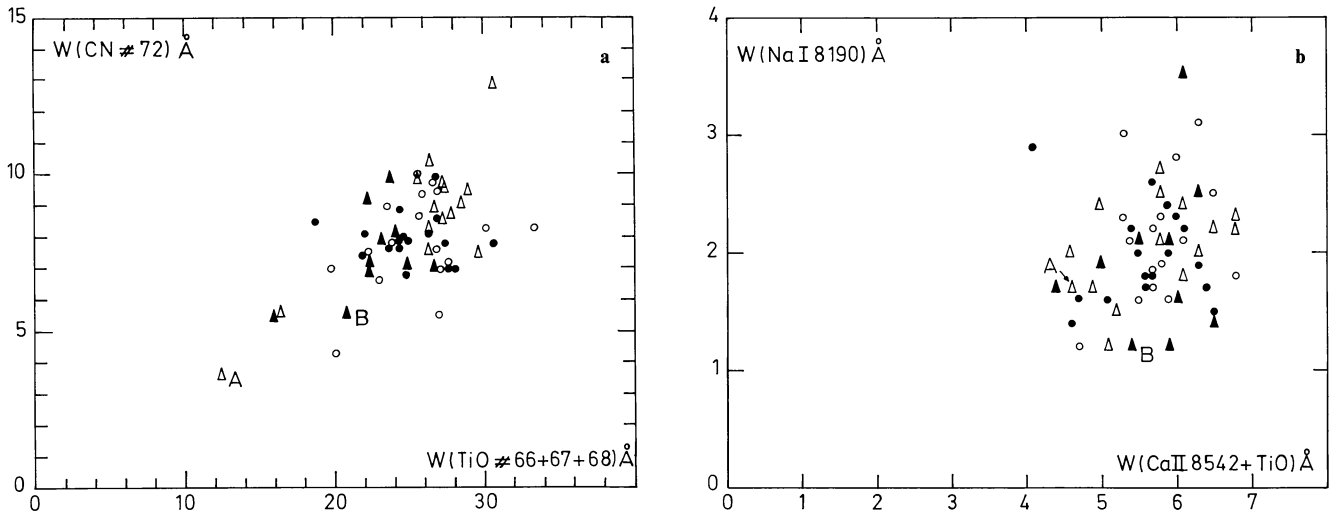


**Fig. 13a and b.** Comparison, of respectively two molecular bands and two metallic lines. Molecular bands present a larger dynamical range of values. Open circles: elliptical galaxies; open triangles: lenticular galaxies; filled circles: Sa and Sb types; filled triangles Sc galaxies

sensitivity of this feature to metallicity. If metallicity effects are present they should be more important for TiO as suggested in Fig. 14b. Only 3 galaxies in our sample have $M_B > -19$ and they are all E or S0 galaxies. One, NGC 4486B, is comparable to its massive counterparts, in terms of $W$ values. This object is the companion of a giant elliptical in the Virgo cluster and thus is possibly tidally stripped (Paper IV and references therein). There is evidence that NGC 3056 is indeed metal deficient with respect to more massive galaxies. Unfortunately, we did not observe in the near-infrared NGC 4476, which in the visible range appeared as a genuine metal-poor galaxy. Because of its position in the metallic feature distributions, NGC 5102 is probably metal deficient. Its weak TiO however may also result from the burst age in this galaxy, 4 $10^8$ yr corresponding to fewer red stars. Indeed, red evolved stars are expected to contribute substantially at two peak values which are $10^7$ and $10^8$ yr, just prior to the burst age in NGC 5102. Spiral galaxies in Figs. 14a and 14b behave like the E and S0 galaxies. This suggests that small bulges in spiral galaxies have a metal content comparable to that in early type galaxies, the total absolute luminosities of the galaxies being the same.

## 6. Conclusions

Main conclusions of the present work are as follows:

1. We present near-infrared CCD spectra with 12.5 Å resolution for 30 star clusters having known ages, metallicities and reddenings. We also observed a sample of 62 nuclei in galaxies of all morphological types. A special attention is given to removal of fringes in this wavelength range.

2. We measure the continuum distribution and the equivalent widths of 13 absorption features for star cluster and galactic nuclei.

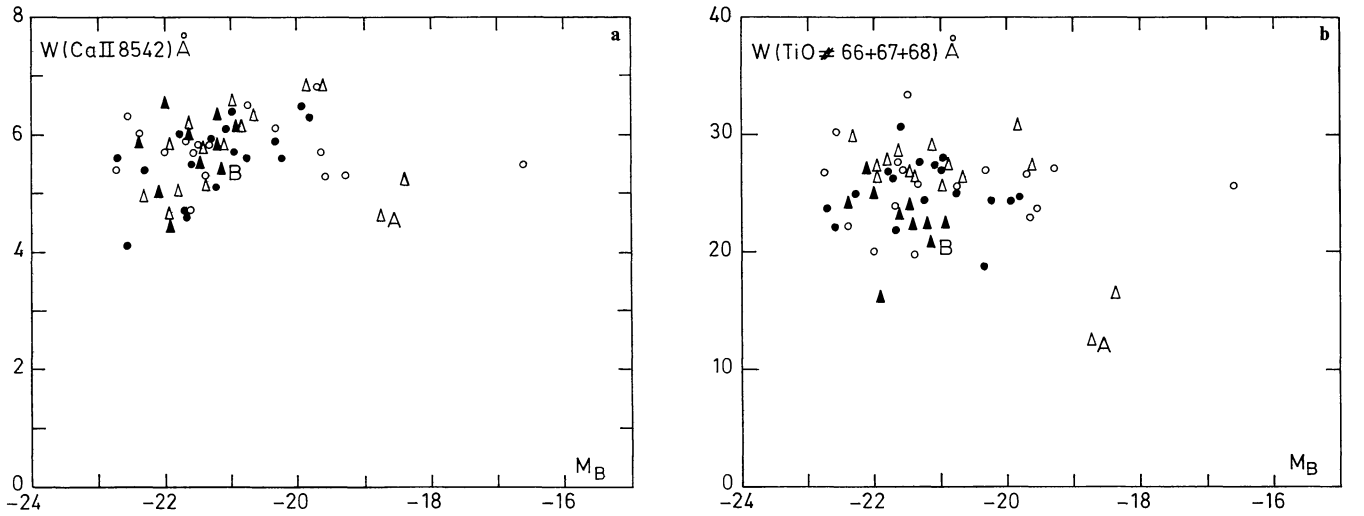


**Fig. 14a and b.** Behaviour of a metallic line (**a**) and a molecular band (**b**) as a function of the galactic absolute magnitude. Same symbols as in Fig. 13

3. Analysis of the star cluster sample shows that in the near-infrared, metallicity is the dominant parameter. Metallic lines present single-valued linear relationship with the metal content while molecular bands tend to depart from linearity at large metallicities. Age effects in blue clusters disturb the relationship for molecular bands.

4. Age produces second order effects of various types: (i) at some particular stages in the evolution of a blue cluster, molecular bands are quite strong owing to the accumulation of luminous red stars, (ii) absorption Paschen lines contaminate some of the metallic windows and, (iii) the continuum slope steepens slightly for young ages.

5. In view of population synthesis of galactic nuclei, we present star cluster grid predictions as a function of age and metallicity for 5 metallic windows and the continuum distribution.

6. Strong-lined globular clusters like NGC 6528 have integrated spectra comparable to those of massive galaxies. Consequently, they are important tools for population synthesis, regardless of their precise metallicity.

7. Strong-lined spectra are observed in the central regions of both spiral galaxies and luminous elliptical galaxies, suggesting a comparable metal content.

8. Even very blue galaxies exhibit, in the near-infrared, spectra quite similar to those observed for the rest of the galaxy sample. However, evidence is found that a large contribution to this range is not from their old underlying population.

## Appendix A

We provide the grid predictions as a function of star cluster age and metallicity for a selection of 5 absorption features and 7 continuum points from Table 1 (Tables A1, A2, A3). We have excluded a number of features for various reasons:

a) molecular windows with strong CN and TiO, owing to a complex behaviour we could not fully model because of our restricted number of data points.

b) CaI + FeI, No. 59, which is rather weak and moreover contaminated in emission line galaxies,

**Table A1.** For Galactic globular clusters, mean relative continuum points at different wavelengths, as a function of metallicity

| | C6630/C5870 | C6990/C5870 | C7520/C5870 | C8040/C5870 | C8408/C5870 | C8700/C5870 | C9100/C5870 |
|---|---|---|---|---|---|---|---|
| [Z/Z⊙] | | | | | | | |
| 0.6 | 0.97±0.05 | 0.99±0.05 | 1.01±0.06 | 1.01±0.07 | 1.03±0.08 | 1.04±0.08 | 1.03±0.09 |
| 0.0 | 0.96±0.05 | 0.96±0.05 | 0.96±0.06 | 0.96±0.07 | 0.96±0.08 | 0.96±0.08 | 0.95±0.09 |
| -0.5 | 0.95±0.05 | 0.94±0.05 | 0.93±0.06 | 0.91±0.07 | 0.90±0.08 | 0.90±0.08 | 0.88±0.09 |
| -1.0 | 0.94±0.05 | 0.91±0.05 | 0.89±0.06 | 0.86±0.07 | 0.84±0.08 | 0.84±0.08 | 0.82±0.09 |
| -1.5 | 0.93±0.05 | 0.89±0.05 | 0.85±0.06 | 0.81±0.07 | 0.78±0.08 | 0.78±0.08 | 0.75±0.09 |
| -2.0 | 0.92±0.05 | 0.87±0.05 | 0.81±0.06 | 0.77±0.07 | 0.72±0.08 | 0.71±0.08 | 0.68±0.09 |

**Table A2.** For intermediate and young clusters, mean relative continuum points at different wavelengths, as a function of age

| | C6630/C5870 | C6990/C5870 | C7520/C5870 | C8040/C5870 | C8408/C5870 | C8700/C5870 | C9100/C5870 |
|---|---|---|---|---|---|---|---|
| age | | | | | | | |
| 5 E9 | 0.96±0.07 | 0.94±0.08 | 0.92±0.09 | 0.88±0.10 | 0.87±0.11 | 0.87±0.12 | 0.85±0.13 |
| E9 | 0.92±0.05 | 0.85±0.05 | 0.81±0.07 | 0.74±0.07 | 0.70±0.08 | 0.70±0.08 | 0.67±0.08 |
| 5 E8 | 0.87±0.04 | 0.80±0.04 | 0.72±0.05 | 0.65±0.05 | 0.61±0.06 | 0.60±0.06 | 0.57±0.07 |
| E8 | 0.81±0.05 | 0.74±0.05 | 0.67±0.06 | 0.61±0.07 | 0.59±0.07 | 0.58±0.08 | 0.54±0.08 |
| 5 E7 | 0.84±0.05 | 0.77±0.05 | 0.73±0.06 | 0.64±0.06 | 0.60±0.07 | 0.61±0.08 | 0.57±0.08 |
| E7 | 0.87±0.11 | 0.80±0.13 | 0.77±0.15 | 0.68±0.17 | 0.65±0.19 | 0.68±0.21 | 0.64±0.25 |

**Table A3.** Mean equivalent widths of five metallic features as a function of metallicity. Being age effects in these windows essentially negligible, the values are valid for clusters of all ages

| | W(#74) NaI | W(#75/6) TiO+TiI | W(#77) CaII 8498 TiO+P16 | W(#78) CaII 8542 TiO+P15 | W(#80) CaII 8662 P13+TiO |
|---|---|---|---|---|---|
| [Z/Z⊙] | | | | | |
| 0.6 | 2.5±0.4 | 16.0±2.9 | 5.0±1.1 | 6.8±1.0 | 6.0±0.9 |
| 0.0 | 2.0±0.4 | 12.3±2.9 | 3.9±1.1 | 5.5±1.0 | 5.0±0.9 |
| -0.5 | 1.6±0.4 | 9.3±2.9 | 3.0±1.1 | 4.5±1.0 | 4.2±0.9 |
| -1.0 | 1.2±0.4 | 6.3±2.9 | 2.2±1.1 | 3.4±1.0 | 3.3±0.9 |
| -1.5 | 0.9±0.4 | 3.2±2.9 | 1.3±1.1 | 2.3±1.0 | 2.5±0.9 |
| -2.0 | 0.5±0.4 | 0.2±2.9 | 0.4±1.1 | 1.2±1.0 | 1.6±0.9 |

c) Hα, No. 60, which was already studied in Papers I and II,

d) P14, No. 79 and P12, No. 81, which, in blue clusters are indicators of the Paschen contamination in the Ca II windows, and, in red clusters and galaxies are rather dominated by molecular absorption,

e) TiO, No. 83 and No. 84, where age and metallicity effects are of an equal weight (Fig. 10) as a result of the presence of P11 and P10 in blue clusters. Contamination from [S III] may be important in emission line galaxies.

The dispersion attached to each value represents the rms differences between $W$ observed in the cluster sample and the grid predictions for 3 age groups: (i) young clusters, (ii) intermediate age clusters and (iii) globular clusters. For blue clusters in particular, where $W$ of molecular bands vary abruptly along the red phases (Sect. 4), these dispersions are large. Although there are strong observational and theoretical evidences that the red phases in blue clusters are real, we do not take them here as age criteria, i.e., using $W$ of strong molecular bands to distinguish populations in small intervals around $10^7$ yr and $10^8$ yr from those outside these age domains. But, indeed, we believe that a *larger* sample of clusters would allow to derive the exact duration of these phases and their dependence on metallicity. This, in turn, would provide important criteria for determining the age and duration of starbursts in blue galaxies, complementary to the best age discriminator, namely the continuum distribution (Paper I).

*Acknowledgements.* We are gratefully indebted to the ESO staff at La Silla and Garching, to the Paris Institute of Astrophysics and to the staff at the Computer Centre in Paris/Meudon Observatory, especially the group who developed the new command system eVe. We thank Dr. H. Spinrad and Dr. G. Cayrel for interesting comments. E.B. thanks the Brazilian Institution CNPq for a fellowship.

**References**

Aaronson, M., Frogel, J., Persson, S.: 1978, *Astrophys. J.* **220**, 442
Baldwin, J., Stone, R.: 1984, *Monthly Notices Roy. Astron. Soc.* **206**, 241
Becker, S., Mathews, G.: 1983, *Astrophys. J.* **270**, 155
Bica, E., Alloin, D.: 1986a, *Astron. Astrophys.* **162**, 21 (Paper I)
Bica, E., Alloin, D.: 1986b, *Astron. Astrophys. Suppl.* **66**, 171 (Paper II)
Bica, E., Alloin, D.: 1987a, *Astron. Astrophys. Suppl.* **70**, 281 (Paper III)
Bica, E., Alloin, D.: 1987b, *Astron. Astrophys.* **181**, 270 (Paper IV)
Bica, E., Dottori, D., Pastoriza, M.: 1986, *Astron. Astrophys.* **156**, 261
Burstein, D., Faber, S., Gaskell, C., Krumm, N.: 1984, *Astrophys. J.* **287**, 586
Carter, D., Visvanathan, N., Pickles, A.: 1986, *Astrophys. J.* **311**, 637
Chiosi, C., Bertelli, G., Bressan, A., Nasi, E., Pigatto, L.: 1985, in *Starforming Dwarf Galaxies*, eds. D. Kunth, T. Thuan, J. Van, Editions Frontières, p. 449
Cohen, J.: 1979, *Astrophys. J.* **228**, 405
Cohen, J.: 1983, *Astrophys. J.* **270**, 654
Faber, S.: 1973, *Astrophys. J.* **179**, 731
Faber, S., French, H.: 1980, *Astrophys. J.* **235**, 405
Frogel, J., Persson, S., Aaronson, M., Mathews, K.: 1978, *Astrophys. J.* **220**, 75
Gratton, R., Quarta, M., Ortolani, S.: 1986, *Astron. Astrophys.* **169**, 208
Jones, J., Alloin, D., Jones, B.: 1984, *Astrophys. J.* **283**, 457
Morgan, W.: 1960, *Astron. J.* **64**, 432
Renzini, A., Buzzoni, A.: 1985, in *Spectral Evolution of Galaxies*, eds. C. Chiosi, A. Renzini, Reidel, Dordrecht, p. 195
Richtler, T., Nelles, B.: 1983, *Astron. Astrophys.* **119**, 75
Sandage, A., Tammann, G.: 1981, *A revised Shapley – Ames Catalogue of Bright Galaxies*, Carnegie Institute of Washington
Spinrad, H.: 1962, *Astrophys. J.* **135**, 715
Spinrad, H., Taylor, B.: 1971, *Astrophys. J. Suppl.* **22**, 445
Turnrose, B.: 1976, *Astrophys. J.* **210**, 33
Zinn, R., West, M.: 1984, *Astrophys. J. Suppl.* **55**, 45